

See discussions, stats, and author profiles for this publication at: <https://www.researchgate.net/publication/262000002>

Discovery of GS-9973, a Selective and Orally Efficacious Inhibitor of Spleen Tyrosine Kinase

ARTICLE in JOURNAL OF MEDICINAL CHEMISTRY · APRIL 2014

Impact Factor: 5.45 · DOI: 10.1021/jm500228a · Source: PubMed

CITATIONS

23

READS

63

17 AUTHORS, INCLUDING:



[Kevin Currie](#)

Gilead Sciences

7 PUBLICATIONS 134 CITATIONS

SEE PROFILE



[Eric B Lansdon](#)

Gilead Sciences

24 PUBLICATIONS 517 CITATIONS

SEE PROFILE



[Julie A Di Paolo](#)

Gilead Sciences

9 PUBLICATIONS 166 CITATIONS

SEE PROFILE



[Scott A Mitchell](#)

Gilead Sciences

26 PUBLICATIONS 807 CITATIONS

SEE PROFILE

Discovery of GS-9973, a Selective and Orally Efficacious Inhibitor of Spleen Tyrosine Kinase

Kevin S. Currie,[†] Jeffrey E. Kropf,[†] Tony Lee,[†] Peter Blomgren,[†] Jianjun Xu,[†] Zhongdong Zhao,[†] Steve Gallion,[‡] J. Andrew Whitney,[‡] Deborah Maclin,[§] Eric B. Lansdon,^{||} Patricia Maciejewski,[‡] Ann Marie Rossi,[‡] Hong Rong,[‡] Jennifer Macaluso,[‡] James Barbosa,[‡] Julie A. Di Paolo,[‡] and Scott A. Mitchell^{*,†}

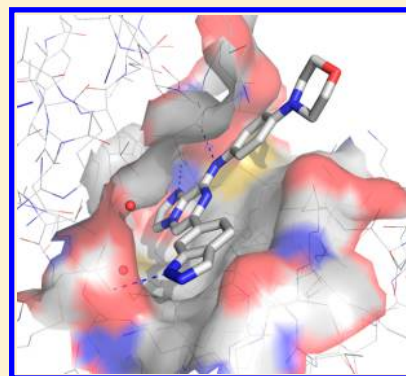
[†]Department of Chemistry, [‡]Department of Biology, and [§]Department of Drug Metabolism, Gilead Sciences, Inc., Branford, Connecticut 06405, United States

^{||}Department of Structural Chemistry, Gilead Sciences, Inc., Foster City, California 94404, United States

[‡]Department of Informatics & Modeling, Atheon Pharma Inc., Waltham, Massachusetts 02451, United States

S Supporting Information

ABSTRACT: Spleen tyrosine kinase (Syk) is an attractive drug target in autoimmune, inflammatory, and oncology disease indications. The most advanced Syk inhibitor, R406, **1** (or its prodrug form fostamatinib, **2**), has shown efficacy in multiple therapeutic indications, but its clinical progress has been hampered by dose-limiting adverse effects that have been attributed, at least in part, to the off-target activities of **1**. It is expected that a more selective Syk inhibitor would provide a greater therapeutic window. Herein we report the discovery and optimization of a novel series of imidazo[1,2-*a*]pyrazine Syk inhibitors. This work culminated in the identification of GS-9973, **68**, a highly selective and orally efficacious Syk inhibitor which is currently undergoing clinical evaluation for autoimmune and oncology indications.



■ INTRODUCTION

Spleen tyrosine kinase (Syk) is a 72 kDa multiple-domain intracellular cytoplasmic tyrosine kinase that is expressed primarily in hematopoietic cells (e.g., B-cells, monocytes, macrophages, mast cells, and neutrophils), where it is recognized as an important mediator of immunoreceptor signaling and has been identified as a potential therapeutic target in allergic, autoimmune, and oncology indications.^{1–3} Immunoreceptor engagement triggers phosphorylation of a pair of tyrosine residues in the cytoplasmic immunoreceptor tyrosine-based activation motifs (ITAMs) by Src family members, and Syk is recruited to the phosphorylated ITAMs via its SH2 domain.^{4–6} Syk critically regulates immune cell function by propagating signaling cascades through phosphorylation of direct targets (such as BLNK/SLP65), leading to activation of downstream pathways, including PI3K, MAPK, Btk, and PLCγ.^{5,7,8} The activation of these pathways in immune cells leads to proliferation, differentiation, cytoskeletal remodeling, and cytokine release. Importantly, since Syk is not expressed in mature T-cells, the immunosuppression that is associated with therapeutics that inhibit T-cell signaling should be avoided.

Rheumatoid arthritis (RA) is a chronic, multifactorial disease that is characterized by the production of autoantibodies, synovial inflammation, pannus formation, and the erosion of cartilage and bone⁹ that manifests itself by marked destruction

and deformation of peripheral joints with a detrimental impact on the quality of life. The underlying mechanisms leading to the disease are not completely understood, but several biologic therapeutics targeting proinflammatory cytokines such as tumor necrosis factor α (TNF α), interleukin-1, and interleukin-6 have had a tremendous impact on its treatment.¹⁰ Despite this therapeutic advance, approximately one-third of all patients fail to respond adequately to these agents or experience treatment intolerance that limits their use.¹¹

The therapeutic potential of Syk inhibition in autoimmune as well as oncology indications has stimulated increased research interest in recent years,^{2,12–14} and several Syk inhibitor chemotypes have been reported (Figure 1), including diaminopyrimidines¹⁵ **1** and **2**, heteroaryl carboxamides^{16–18} **3–5**, aminopyrimidine¹⁹ **6**, and naphthyridine²⁰ **7**. Several of these compounds have demonstrated efficacy in animal models of inflammation. Compounds **2** and **3** dose-dependently inhibited disease scores and suppressed joint inflammation and bone erosion in rodent models of arthritis.^{15,16,21} Compound **4** is reported to be a highly selective Syk inhibitor and was efficacious in the rat reversed passive arthus (RPA) model of inflammation.¹⁷ Preclinical studies with **1**, or its prodrug **2** (R788, fostamatinib), have demonstrated efficacy in

Received: February 18, 2014

Published: April 6, 2014

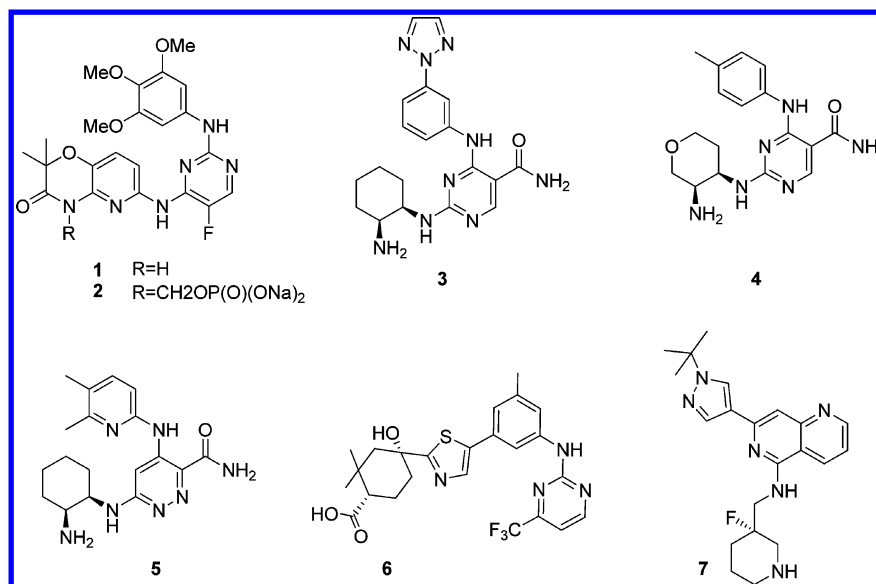
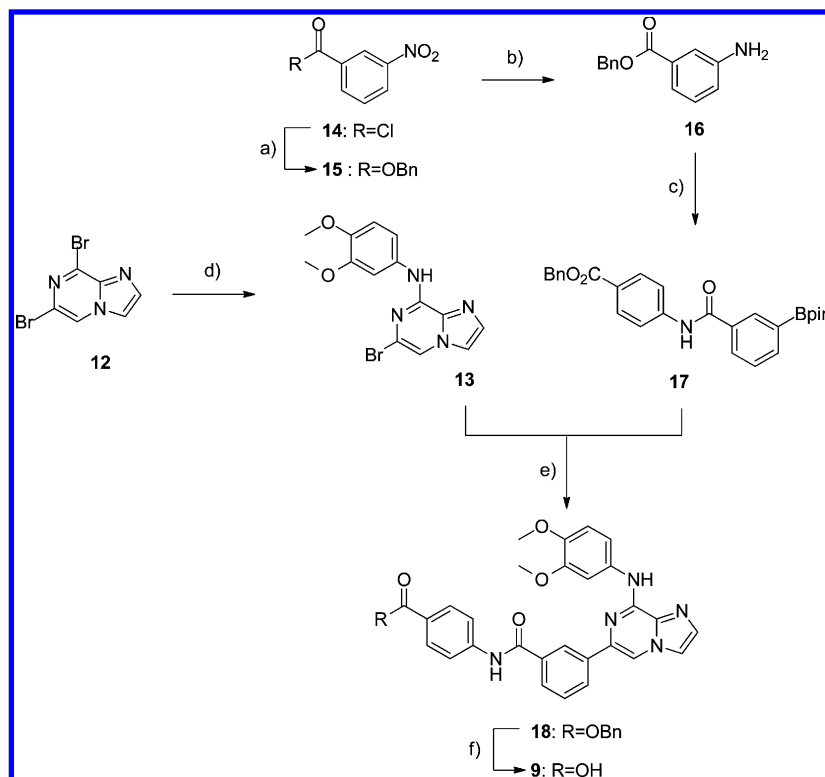


Figure 1. Syk inhibitor chemotypes.

Scheme 1^a

^aReagents and conditions: (a) benzyl alcohol, Et₃N, CH₂Cl₂, rt, 22 h; (b) Fe powder, EtOH, H₂SO₄, H₂O, 60 °C, 90 min; (c) 3-(4,4,5,5-tetramethyl-1,3,2-dioxaborolan-2-yl)benzoyl chloride, DIPEA, CH₂Cl₂, rt; (d) 3,4-dimethoxyaniline, DIEA, IPA, 100 °C, 22 h; (e) Pd(PPh₃)₄, Na₂CO₃, 1,4-dioxane, H₂O, reflux, 2.5 h; (f) Pd/C, H₂, EtOH, EtOAc, 30 min.

several additional animal models of autoimmune/inflammatory disease, including systemic lupus erythematosus (SLE),^{22,23} nephrotoxic nephritis,²⁴ autoimmune diabetes,²⁵ idiopathic thrombocytopenia purpura (ITP),²⁶ autoimmune hemolytic anemia (AHA),²⁶ and asthma.^{27,28} Furthermore, **2** has shown activity in various B-cell leukemia and lymphoma models.^{29–31}

Fostamatinib has been evaluated in several phase II RA studies,^{32–35} where it has demonstrated dose-dependent efficacy as measured by reduction in ACR20 and ACR50

scores. However, gastrointestinal upset, neutropenia, and hypertension were commonly occurring adverse effects. The adverse events seen in the initial TASKI trial have prohibited the use of the most efficacious dose (150 mg bid) in subsequent RA studies, and fostamatinib failed to meet primary efficacy end points in some of these trials.^{33,36–38} Additional clinical trials in B-cell malignancies,³⁹ ITP,²⁶ and solid tumors^{40,41} have been reported with promising efficacy results, but with a similar adverse effect profile. It appears that the dose-

limiting adverse effects of **2** have restricted the ability to achieve maximum efficacy and may limit its clinical application in chronic indications such as RA. The adverse event profile of **2** has been putatively attributed to the poor kinase selectivity of its parent compound **1** (R406).^{42,43}

Together, these data validate the therapeutic potential of Syk inhibition in autoimmune and oncology indications and highlight the need for compounds with improved safety profiles. A key advantage of such compounds would be the ability to achieve levels of in vivo Syk inhibition that are not currently achievable due to dose-limiting toxicities. Accordingly, we sought to identify Syk inhibitors with significantly improved selectivity profiles over **1**. Herein we describe the discovery of GS-9973, a selective and orally efficacious imidazopyrazine-based Syk inhibitor that has the potential for an improved efficacy and tolerability in patients.

SYNTHESIS

Our initial lead compound **9** was prepared as shown in Scheme 1. Commercially available 3,4-dimethoxyaniline regioselectively displaced the 6-bromide of 6,8-dibromoimidazo[1,2-*a*]pyrazine (**12**), which was either purchased or synthesized according to the literature procedures, to provide the bromide intermediate **13** in high yield.⁴⁴ Reaction of 3-nitrobenzoyl chloride with benzyl alcohol followed by the iron-mediated reduction of the nitro group gave aniline **16**, which was acylated to afford the corresponding boronic ester **17**. Subsequent Suzuki–Miyaura coupling reaction of **13** with the boronic ester **17** afforded **18**, which was then debenzylated by hydrogenolysis to provide **9**. All of the analogues in Table 1 were prepared analogously from variously substituted anilines.

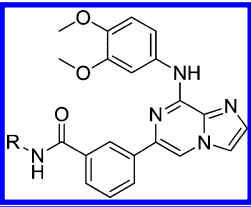
The syntheses of disubstituted coupling partners **21e–l** for the analogues described in Table 2 are shown in Scheme 2. Commercially available *m*- and *p*-benzoic acids were efficiently converted to the corresponding amides **20e–k** by treatment with amines in the presence of pyBOP or EDCI. Then **20e–l** were transformed to boronic esters **21e–l** using a catalytic amount of PdCl₂(dppf). It was important to apply an excess amount of bis(pinacolato)diboron to ensure a complete consumption of **20e–l** to provide **21e–l** in good yields.

The bicyclic heteroaromatic analogues described in Table 3 were prepared using the route exemplified by compound **24** in Scheme 3. From the commercially available bromide **22**, the boronic ester **23** was synthesized in one step, and Suzuki–Miyaura coupling reaction with the intermediate **13** afforded **24** in good yield. All boronic esters used to prepare the compounds in Table 3 were either purchased or synthesized using the procedures described above.

The synthesis of **30** (Scheme 4) exemplifies the route to the compounds in Table 4. An S_NAr reaction between 1-fluoro-4-nitrobenzene (**25**) and 4-methylpiperidin-4-ol followed by nitro reduction gave aniline **27** in good yield. Next, aniline **27** was combined with 6,8-dibromoimidazo[1,2-*a*]pyrazine (**12**) in the presence of *N,N*-diisopropylethylamine to provide the bromide **28**, which was further converted to **30** by coupling reaction with indazole boronic ester **29**. This general route was utilized for preparation of the compounds in Table 4.

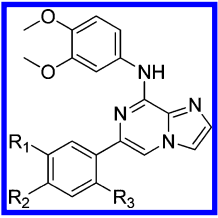
The initial synthetic steps of the pyran derivative **70** are shown in Scheme 5. Friedel–Crafts alkylation of benzene with chloropyran **31** gave phenylpyran **32**, which underwent nitration with nitric acid to provide **33**. Compound **70** was then prepared by the procedure described in Scheme 4.

Table 1. Optimization of the D-Ring Acid of **9**



Analog	R	Syk (nM)	pBLNK (nM)
9	HOOC-	0.84	175
34	MeOOC-	15.2	293
35	HOOC-	8.9	643
36	HOCH ₂ CO-	2.6	2165
37	H ₂ NOC-	4.3	105
38	MeO ₂ SHNOC-	2.2	824
39		1.5	308
40		16.5	199
41		11.7	166
42		11	270

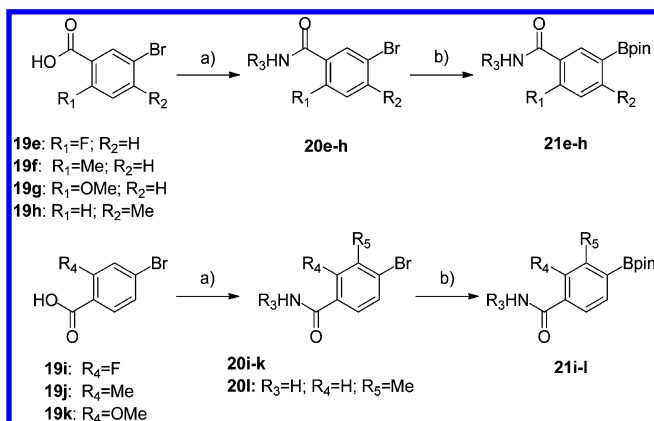
Table 2. Optimization of C-Ring Carboxamides



analogue	R ₁	R ₂	R ₃	[Syk] (nM)	[pBLNK] (nM)
11	CONH ₂	H	H	27.1	244
43	H	CONH ₂	H	17.7	127
44	CONHMe	H	H	50.2	619
45	CONMe ₂	H	H	112	615
46	CONH ₂	F	H	67.3	248
47	CONH ₂	Me	H	28.3	123
48	CONH ₂	OMe	H	37.4	268
49	CONH ₂	H	Me	466	
50	F	CONH ₂	H	18.6	134
51	Me	CONH ₂	H	64.1	310
52	OMe	CONH ₂	H	23.8	251
53	H	CONH ₂	Me	113	418

RESULTS AND DISCUSSION

Screening of our compound library identified compound **8** (Figure 2), which was found to have promising activity in a Syk enzyme assay (IC₅₀ = 65 nM). Early work replaced the *tert*-butylphenyl group with dimethoxyphenyl (based on the structures of **1** and Bayer's Syk inhibitor BAY 61-3606)⁴⁵ and reversed the amide to provide our initial lead compound **9**,

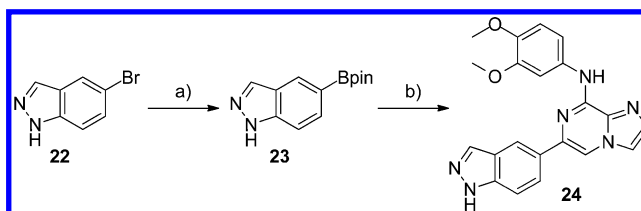
Scheme 2^a

^aReagents and conditions: (a) PyBOP, NH₄Cl, NMM, DMF or EDCI, HOBT, NH₄OH, NMM, THF; (b) B₂(pin)₂, KOAc, [PdCl₂(dppf)]·CH₂Cl₂, 1,4-dioxane.

Table 3. C-Ring Optimization with 5,6/6,6-Heterocycles

Analogue	R	Syk (nM)	pBLNK (nM)	CD63 (nM)
54		2.7	94	2788
55		3.8	24	919
56		6.3	139	2776
57		12.6	151	6450
58		8.6	86	
24		10.4	122	
59		12.3	136	1003
60		20.9	183	6797
61		2.3	57	2198
62		33.4	168	
63		4.7	62	1483

which possessed excellent Syk potency of 0.8 nM (Table 1). When screened at 10 μ M against 317 kinases in the KinomeScan competition binding assay,^{46,47} **9** bound to only eight kinases, including Syk, with an $S(10)$ score of 0.03 [$S(10)$ is defined as the (number of kinases with a control score of

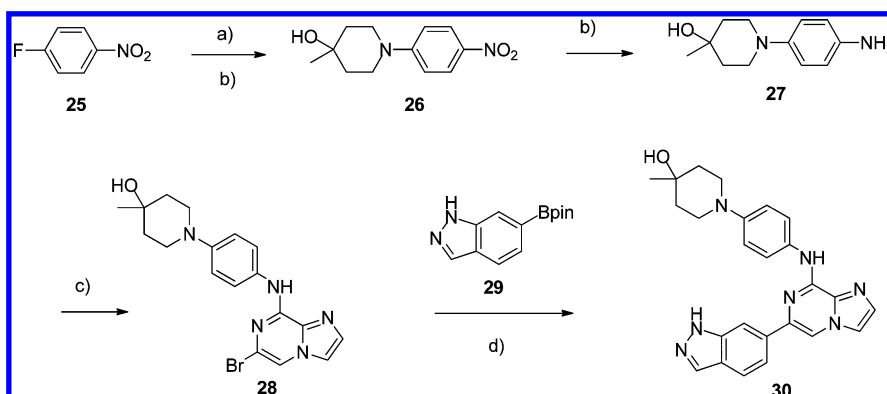
Scheme 3^a

^aReagents and conditions: (a) B₂(pin)₂, KOAc, [PdCl₂(dppf)]·CH₂Cl₂, DMSO, 90 °C, 16 h; (b) bromide **12**, Pd(PPh₃)₄, Na₂CO₃, 1,4-dioxane, H₂O, microwave, 125 °C, 20 min.

<10%)/(total number of kinases)]. Dose–response follow-up showed a K_d for Syk binding of 4 nM. In contrast, **1** bound 215 out of 358 kinases with an $S(10) = 0.60$ and had a Syk K_d of 12 nM. The promising selectivity profile of **9** prompted us to initiate a medicinal chemistry program in the imidazopyrazine series.

To guide the initial medicinal chemistry efforts, we obtained an X-ray crystal structure of **9** bound to the kinase domain of Syk. **9** was found to occupy the ATP binding pocket (Figure 3), with N-1 of the imidazopyrazine system accepting a hydrogen bond from the backbone NH of A451, while the aniline NH of **9** forms a second H-bond with the carbonyl group of the same residue. The aniline ring (A-ring) extends toward the solvent and forms contacts with L377, G454, and P455. The phenyl ring at the 6-position (C-ring) sits above the gatekeeper M448 and near the catalytic K402 side chain and also forms extensive van der Waals contacts with V385 in the P-loop. The amide linker is slightly twisted and forms a hydrogen bond to a water molecule in the pocket. The terminal phenyl ring (D-ring) is oriented up toward the top of the pocket, enabling van der Waals contacts with the side chains of P455 and R498, and positions the carboxylic acid to form a hydrogen bond with N457 and a water molecule.

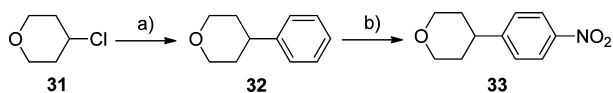
Despite the potent inhibition of Syk enzymatic activity, **9** suffered a 200-fold loss in cellular potency as measured by BCR-mediated phosphorylation of BLNK (pBLNK) in Ramos cells and also exhibited poor activity in a human whole blood assay measuring inhibition of Fc ϵ R-mediated basophil degranulation ($EC_{50} > 5 \mu$ M). We suspected the benzoic acid moiety as a contributor to these observations, so our initial SAR investigations focused on modifying this region of the molecule (Table 1). The *m*-CO₂H analogue **35** and phenylacetic acid derivative **36** lost 10-fold and 3-fold enzyme potency relative to **9** but still retained single-digit nanomolar activity. Modeling showed that it would be difficult for the carboxylic acid to maintain an optimal interaction with N457 in both these analogues while preserving the network of other favorable contacts. Due to the presence of multiple attractive interactions, the specific contact with N457 is likely to be beneficial but not critical for potent Syk inhibition. Consistent with this, the methyl ester analogue **34**, while 20-fold less potent compared to the acid, still retained an IC_{50} of 15 nM. A number of carboxylic acid bioisosteres^{48–50} and alternative hydrogen bond donating groups were investigated in an effort to improve cellular potency. The tetrazole **39** and acylsulfonamide **38** analogues retained enzymatic potency comparable to that of **9**, but failed to improve cellular potency. The reduced enzyme–cell shift (10–27-fold) of the primary amide **37** and the heterocyclic derivatives **40–42** was encouraging, but we felt that further improvements in cellular potency were required.

Scheme 4^a

^aReagents and conditions: (a) 4-methylpiperidin-4-ol hydrochloride, DIEA, CH₃CN, reflux, 2.5 h; (b) 10% Pd/C (wet), H₂ gas (1 atm), ethanol; (c) 6,8-dibromoimidazo[1,2-*a*]pyrazine, DIPEA, IPA, reflux, 2 h; (d) Pd(PPh₃)₄, Na₂CO₃, 1,4-dioxane, H₂O, microwave, 135 °C, 35 min.

Table 4. A-Ring Substituent Optimization

Analog	R1	R2	Syk (nM)	pBLNK (nM)	CD63 (nM)	HLM Cl (L/hr/kg)
64	H	H	26.8	>3300		0.49
65	H	OMe	8.5	374		
66	OMe	H	7.0	161		
67		H	3.9	80	1258	
30		H	1.4	15	677	0.27
68		H	7.7	26	367	0.41
69		H	2.1	40	>10000	0.60
70		H	3.8	2366	>10000	0.12
71		H	7.6	42	1093	
72		H	23.1	73		0.30
73		OMe	0.44	20	353	0.75

Scheme 5^a

^aReagents and conditions: (a) AlCl₃, benzene, 0 °C to rt (*caution: gas evolution!*), 1 h, 92%; (b) AcOH, H₂SO₄, HNO₃, rt, 30 min.

It became apparent that the relatively high molecular weight and lipophilicity of this series would constrain further

optimization of cellular and whole blood potency. Subsequent to our work, similar problems in a series of imidazopyridazine Syk inhibitors have recently been described (10, Figure 2).⁵¹ We therefore sought to truncate the molecule to identify a more druglike template for further chemistry efforts. We found that removal of the benzoic acid moiety resulted in Syk IC₅₀ values of 27 and 18 nM for the *m*- and *p*-carboxamides 11 (Figure 4) and 43, respectively. Despite the order of magnitude loss in Syk enzyme potency, both of these compounds had enzyme–cell shifts of less than 10-fold, suggesting that the

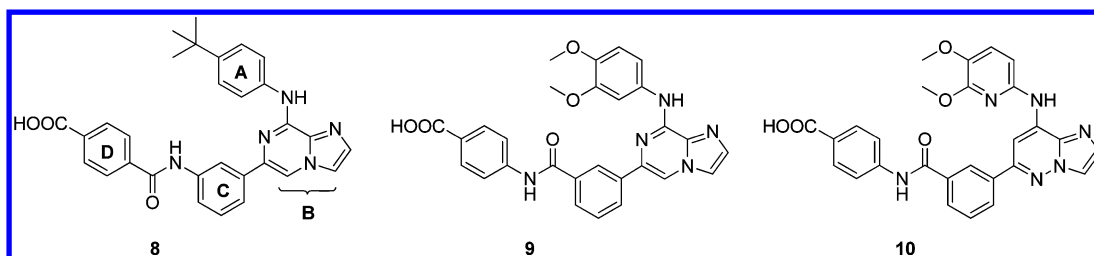


Figure 2. Initial hit 8, lead 9, and Roche extended acid 10.

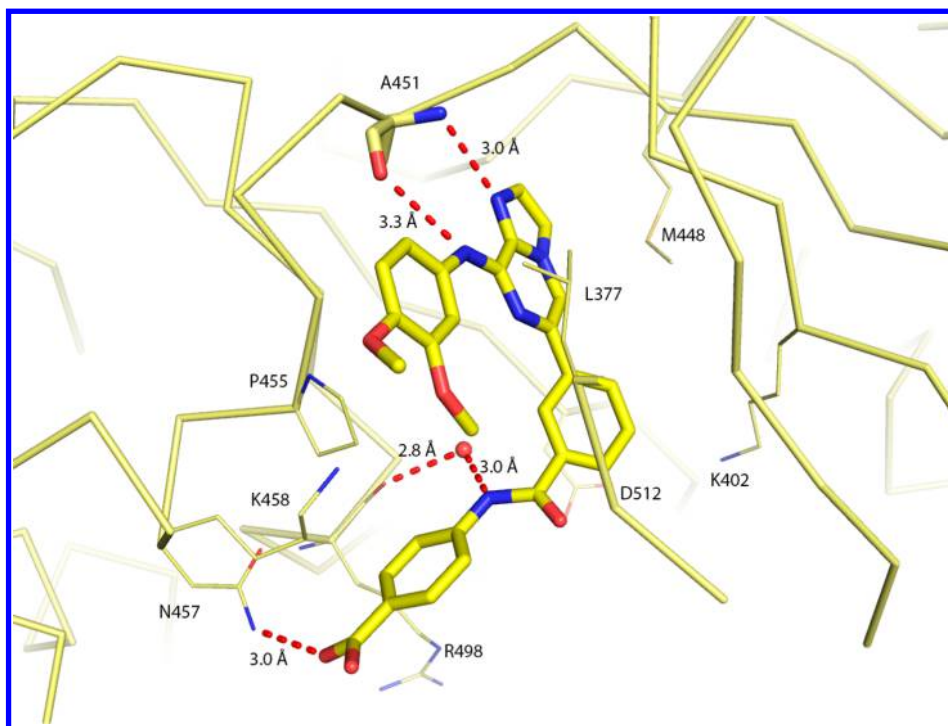


Figure 3. Cocrystal structure (2.0 Å) of the Syk kinase domain with compound 9 (PDB code 4PV0). Dashed lines show hydrogen bond contacts in the pocket between the compound and protein. Part of the P-loop is removed to make viewing the compound binding mode easier.

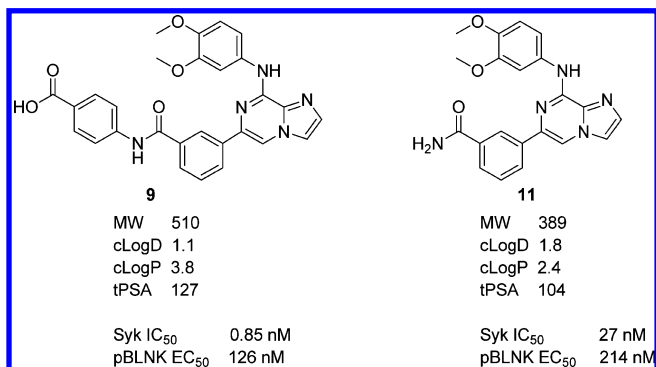


Figure 4. Results of truncation.

reduction in molecular weight (24%) and log *P* (1.4 units) had indeed improved the molecular properties. Furthermore, **43** showed encouraging bioavailability (22%) in the rat after oral dosing at 10 mg/kg. Considering the in vivo clearance (Cl = 3.05 L/h/kg), the bioavailability for **43** is indicative of good absorption from the gastrointestinal (GI) tract. Importantly, truncation to the primary amide did not significantly erode kinome selectivity, as the *S*(10) scores for compounds **11** (0.05) and **43** (0.04) were comparable to that of the lead

compound **9** (0.03). This selectivity profile coupled with the improved molecular properties encouraged us to further explore the truncated series, with the goal of improving intrinsic potency.

The results of our SAR studies around the C-ring phenylcarboxamide are summarized in Table 2. In both the 3- and 4-carboxamido series, addition of small substituents *ortho* to the carboxamide (compounds **46–48** and **50–52**, respectively) had little impact on Syk enzyme potency and failed to improve upon the parent compound **11** or **43**. In contrast, addition of a methyl group *ortho* to the phenyl–imidazopyrazine linkage reduced potency significantly in both cases (**49** and **53**). Energy minimizations with the Merck molecular force field (MMFF) indicate that this methyl group increases the dihedral angle between the phenyl ring and the imidazopyrazine from 42° to 70°. It is possible that this twist disrupts potential H-bond interactions between the carboxamide and the protein and also erodes productive interactions between the phenyl ring and V385. The importance of this H-bonding interaction is supported by the reduced potency of the mono- and dimethyl amides **44** and **45**, which suffered 2- and 6-fold reductions in Syk potency, respectively. The data in Table 2 suggested that there was little potency advantage to be gained by substitution of the phenyl ring and that manipulating

the trajectory of the NH to the enzyme could be a more productive strategy.

Incorporating the NH into a ring system consistently improved Syk potency relative to that of the carboxamides (Table 3). The indole and indazole analogues **54** and **55** improved activity by 5–10-fold over the carboxamide analogues **11** and **43** (Table 2). The benzimidazole and benzotriazole analogues **56** and **57** showed a slight reduction in potency relative to the corresponding indole and indazole, possibly due to the existence of tautomeric forms in the former ring systems that are less compatible with potent Syk binding. The isomeric 5-indole and 5-indazole isomers **58** and **24** exhibited Syk IC_{50} values 3–4-fold weaker than their 6-substituted counterparts **54** and **55**, indicating a preference for the *m*-NH (relative to the imidazopyrazine core). The importance of the free NH for potent inhibition was further confirmed by the weaker enzyme and cellular activity of the *N*-methyl derivatives **59** and **60**. We also examined 6,6-semisaturated ring systems and found the same preference for a *m*-NH (relative to the imidazopyrazine core) versus the *para* regioisomer (**61** vs **62**). The lactam **61** and its reduced benzomorpholine analogue **63** had potency comparable to that of the indazole, indicating that the NH can be presented in a variety of contexts to form favorable hydrogen bond interactions with the enzyme.⁵² Several compounds in Table 3 demonstrated potent cell-based activity in the pBLNK assay, but still failed to produce satisfactory whole blood potency. Only the indazole analogue **55** had an EC_{50} of less than 1 μ M in whole blood, and this compound was profiled further. When screened against 359 kinases at 10 μ M, **55** produced an $S(10)$ score of 0.08. Further analysis of the top 39 hits from the primary screen showed that **55** did not bind to any kinases with potency within 10-fold of that of Syk ($K_d = 9$ nM). Thus, significant truncation of the initial lead compound **9** led to improved cellular and whole blood potency with no appreciable loss in selectivity.

In a rat pharmacokinetic (PK) study, **55** showed moderate clearance (2.1 L/h/kg) with encouraging oral bioavailability (36%) when dosed at 10 mg/kg. However, the metabolic stability in human liver microsomes was unacceptable, with a predicted clearance of 0.72 L/h/kg. We suspected the dimethoxyphenyl motif as a metabolic liability, so the next phase of our investigation focused on this region of the molecule (Table 4). Crystallographic information suggested that the 4-position of the phenyl ring offered a trajectory toward solvent, and we anticipated this would provide a platform to improve the absorption, distribution, metabolism, and excretion (ADME)/PK properties without adversely affecting Syk binding. Compounds **55** and **64–66** confirmed that the 3,4-dimethoxy arrangement was optimal for enzyme potency. The monomethoxy derivatives **65** and **66**, despite retaining Syk activity within 2-fold of the dimethoxy compound **55**, suffered a 7–15-fold loss in cellular potency. In contrast, monosubstitution of the *para* position with a variety of aliphatic amines (**30**, **67–69**, **71–73**) retained pBLNK potency within 1–3-fold of that of **55**. Consistent with the presumed metabolic liability of the dimethoxyphenyl group, many of these analogues also improved metabolic stability in human liver microsomes. In particular, the 4-methyl-4-hydroxypiperidine **30** exhibited a predicted human clearance of 0.27 L/h/kg and excellent enzymatic potency, although the whole blood EC_{50} remained above 500 nM. However, the morpholine derivative **68** provided a good balance of whole blood potency and metabolic stability, and we prepared several close analogues of this

compound to optimize these parameters further. To test the role of the morpholine nitrogen, we synthesized the pyran analogue **70** and found a significant improvement in microsomal stability, but this compound had surprisingly poor cellular activity. Reduced potency was also seen with the ring-opened **71** or ring-expanded **72** morpholine analogue. Finally, having previously demonstrated improved enzymatic potency of the dimethoxy relative to the monomethoxy arrangement, we prepared the 3-methoxy-4-morpholino derivative **73**. While intrinsic and cellular potencies were improved, this did not translate to improved activity in the whole blood assay. Furthermore, introduction of the methoxy group reduced the metabolic stability significantly. At this stage of our optimization, **68** was selected for further evaluation.

The crystal structure of **68** bound to the Syk kinase domain (Figure 5A) shows that the aminoimidazopyrazine core

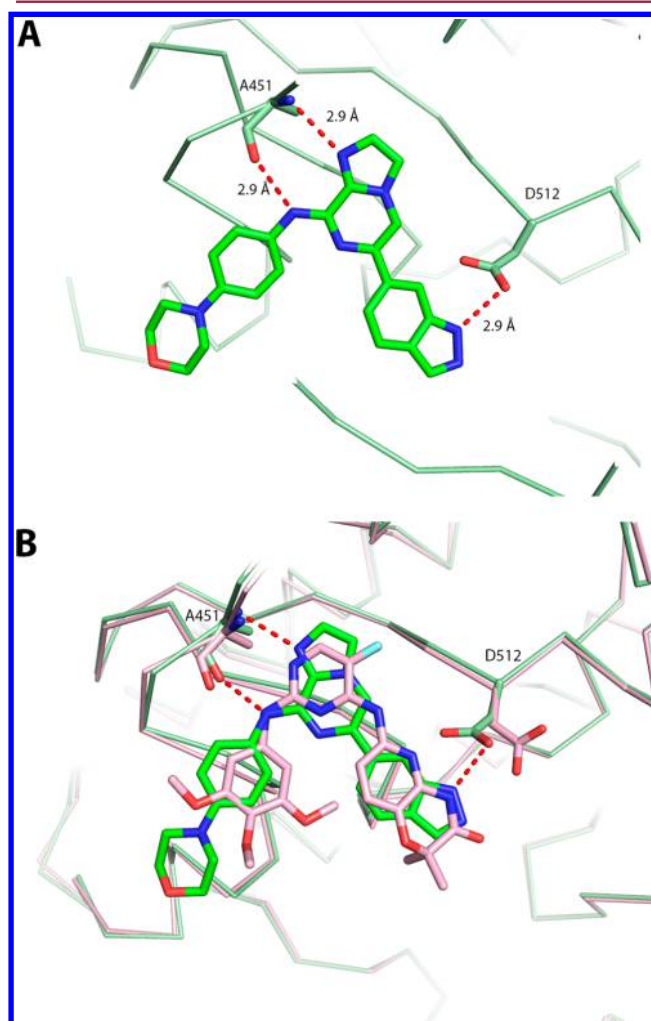


Figure 5. (A) Cocrystal structure (2.1 Å) of Syk with compound **68** (PDB code 4PUZ). Along with the hinge interactions, **68** forms a new hydrogen bond with D512. (B) Comparison of the binding modes between **68** (green) and **1** (pink).

maintains the same hinge interactions observed with **9**. The 4-morpholino group extends beyond the hinge residues toward solvent. Surprisingly, a significant conformational difference in the C-ring between **9** and **68** was observed. The C-ring phenyl of **9** rotates 27° relative to the core, whereas the indazole system of **68** is rotated 24° in the opposite direction. This

Table 5. ADME Profile of 68 in Multiple Species

species	microsomal half-life ^a (min)	predicted hepatic Cl ^a (L/h/kg)	Cl ^b (L/h/kg)	V _{ss} ^b (L/kg)	F ^c (%)	plasma protein binding ^c (%)	Caco-2 P _{app} ^d (10 ⁻⁶ cm/s)
rat	35	1.53	0.27 ± 0.01	0.52 ± 0.05	67 ± 9	99.2	A/B 3.20, B/A 1.95
dog	23.4	0.85	0.80 ± 0.03	1.41 ± 0.40	53 ± 16	92.8	
human	98.6	0.29				97.1	

^aFrom hepatic microsomes. ^bIntravenous dose of 0.4 mg/kg. ^cOral dose of 1 mg/kg. ^dAt 5 μ M concentration.

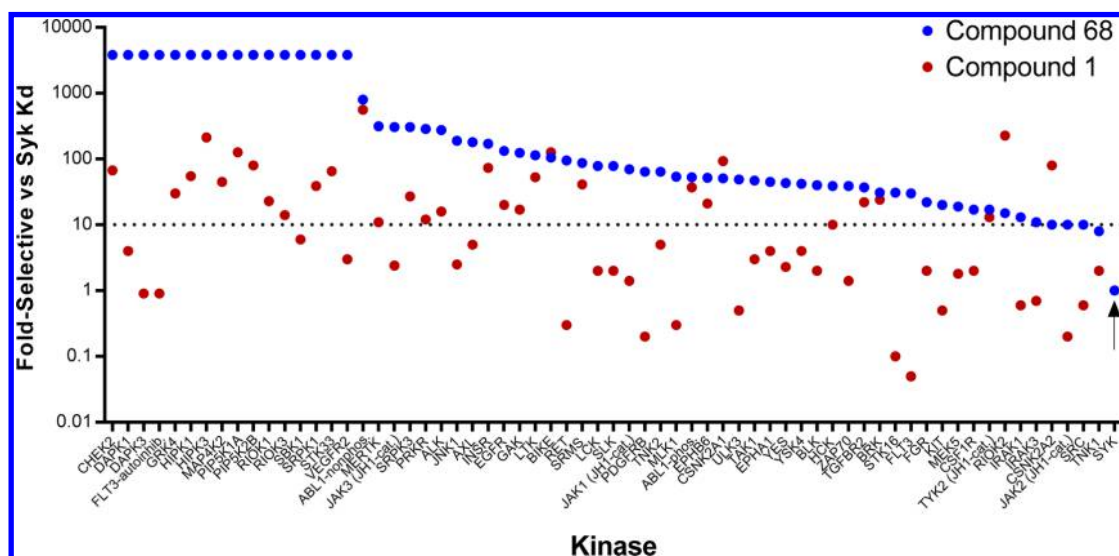


Figure 6. K_d analysis of 68 and 1. Individual kinases for which K_d values were determined are arranged in descending order of selectivity of 68 on the x-axis. Fold selectivities for inhibition of each kinase relative to the Syk K_d for 68 (blue dots) and 1 (red dots) are shown.

Table 6. Biological Profile of GS-9973

target	cell type	stimulation	readout	EC ₅₀ ± SD (nM)	
				GS-9973	R406
Syk	Ramos	α IgM	pBLNK	26	53 ± 32
Jak2	TF-1	EPO	pStat5	453 ± 335	13 ± 1.5
ckit	BMMCs	SCF	cKit	445 ± 100	46 ± 11
Flt3	MV4,11	na	proliferation	327 ± 175	10 ± 5
Ret	SK-N-MC		pRet	>1000	36 ± 9
KDR	HUVEC	VEGF	pVEGFR2	>1000	36
Syk	B-cell	α IgM	CD86	125 ± 78	335 ± 36
	B-cell	α IgM	proliferation	41 ± 27	151 ± 109
	monocytes	immune complex	TNF α production	147 ± 16	na
	basophils (WB)	α IgE	CD63	387 ± 220	3659 ± 2116

difference in rotation brings the NH of the indazole closer to the DFG motif. The D512 side chain rotates toward the indazole NH and forms a hydrogen bond, which explains the intrinsic potency of 68 even without the network of additional interactions, including the H-bond to N457 that is evident in the more elaborate structure 9.

The in vitro ADME and in vivo PK properties of 68 are summarized in Table 5. 68 is highly protein bound across species, with a human free fraction of 2.7%. 68 was relatively stable in human liver microsomes (predicted Cl = 0.29 L/h/kg) but was less stable in preclinical species. In vivo, the clearance relative to hepatic blood flow was low in rat but was higher in dog, with dog having a relatively lower extent of protein binding. 68 showed good bidirectional permeability across Caco-2 cell monolayers, indicating good absorption potential and low potential for efflux at concentrations likely to be achieved clinically. When dosed orally at 1 mg/kg in solution,

68 showed moderate to high bioavailability in rat and dog. A comparison of the bioavailability and hepatic extraction in these species indicates that the extent of absorption from the GI tract is high (>75%). Since inhibition of metabolizing enzymes has the potential to cause clinically relevant drug–drug interactions, we evaluated the ability of 68 to inhibit CYP1A2, 2C9, 2C19, 2D6, and 3A4. IC₅₀ values were >10 μ M in all cases. The solubility of crystalline 68 in simulated intestinal fluid under both fed and fasted conditions was quite low (16 and 2 μ M, respectively), most likely due to its high crystallinity and melting point (326 °C).

Maintaining a high degree of kinase selectivity was paramount in our program, and 68 was initially profiled using the KinomeScan platform against a panel of 359 nonmutant kinases at a single concentration of 10 μ M. The resulting S(10) scores showed dramatically improved selectivity compared to that of 1 [S(10) = 0.12 and 0.60, respectively]. To characterize

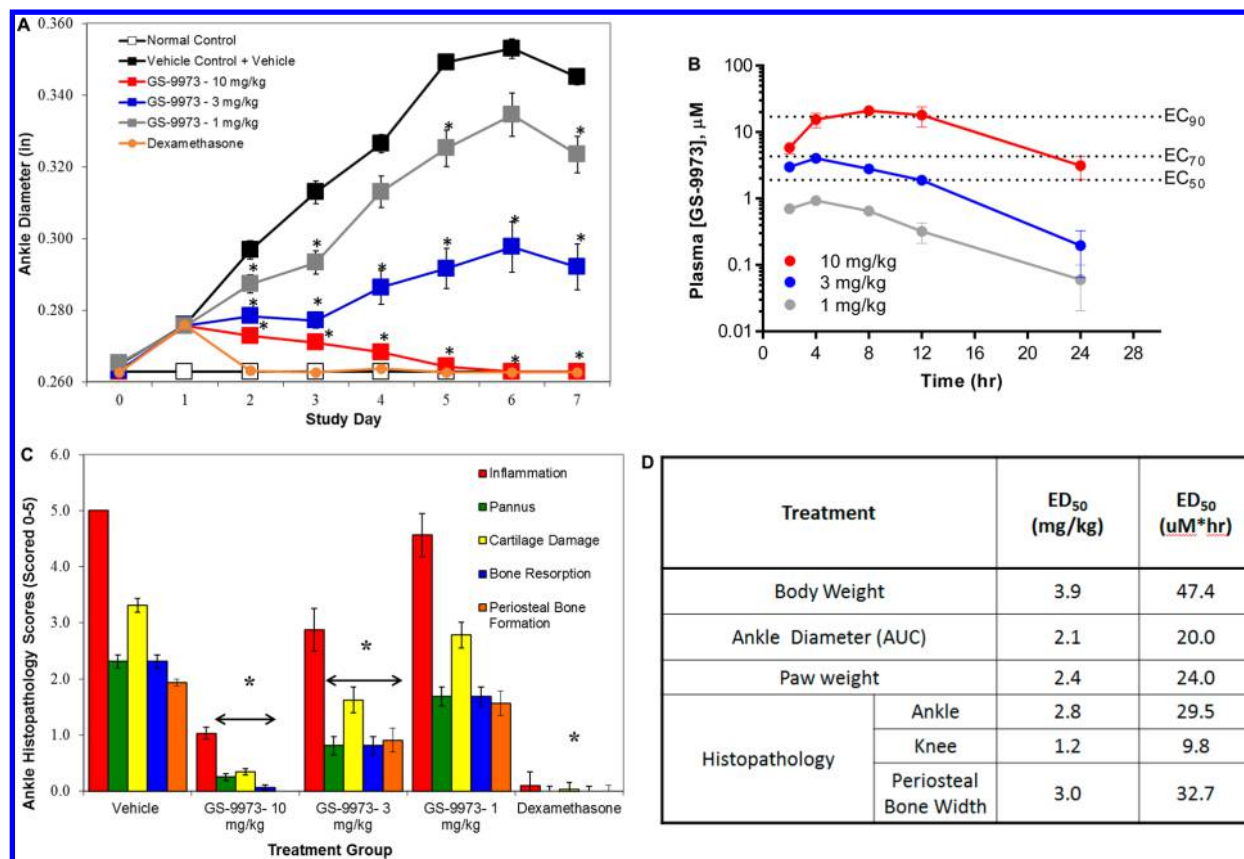


Figure 7. GS-9973 was efficacious in rat established collagen-induced arthritis. Collagen-induced arthritis was initiated in rats as described in the Experimental Section. Twice daily oral dosing with vehicle or GS-9973 was commenced at disease onset on day 10 or 11 (study day 1). Calipers were used to measure ankle thickness daily (mean \pm SEM; an asterisk indicates $p < 0.01$ vs arthritis + vehicle) (A). Blood plasma compound PK was assessed following the final dose (B). On the basis of histological evaluation of ankle sections by hematoxylin and eosin (H&E) staining and a five-point scale described in the Experimental Section, robust disease-modifying antirheumatic drug (DMARD) activity of GS-9973 was observed (C). ED₅₀ and EC₅₀ values for GS-9973 were calculated for multiple measured disease parameters (D).

the selectivity profile in more detail, K_d values were determined for 67 kinases, including all those that showed control scores of $<10\%$ in the primary screen, and were compared to the corresponding K_d values for **1** (Figure 6). Only 1 kinase, TNK1, showed less than 10-fold selectivity versus Syk for **68**, whereas **1** bound 36 kinases within 10-fold of the potency of Syk and 14 kinases more potently than Syk. Additional K_d values were determined for **1** on the basis of the primary screen data, and additional kinases with K_d values more potent than that of Syk were identified (Supplementary Table 1, Supporting Information). We selected five kinase targets for further cellular profiling on the basis of their potential to confound efficacy readouts or contribute to clinically observed safety issues with **1**. The results showed that, in cells, **68** inhibited Flt3, Jak2, c-Kit, KDR, and Ret activity 10–35-fold less potently than **1**. **68** showed 13- to >1000 -fold cellular selectivity for Syk as assessed by target protein phosphorylation or functional response (Table 6), whereas **1** inhibited four out of five of these kinases more potently than Syk. Together these results demonstrated the excellent selectivity profile of **68** and highlighted the potential for an improved clinical safety margin.

As a potential rationale for this improved selectivity, Figure 5B shows a superposition of the crystal structures of **68** and **1** bound to Syk,⁵³ indicating the similar binding pose of both. We hypothesize that the flexibility provided by the extra rotatable bond in **1** allows it to adopt conformations that can interact with several kinases in addition to Syk. For example, inhibition

of VEGFR2 by various conformations of the diaminopyrimidine scaffold has been described.⁵⁴ We believe that **1** potentially inhibits VEGFR2 by adopting one or more of these active conformations, which are not accessible to the more conformationally restricted **68**.

Having demonstrated the high selectivity of **68** for Syk, we tested its ability to inhibit multiple cellular functions that contribute to the pathology of RA (Table 6). In vitro, **68** potentially inhibited BCR-mediated activation and proliferation of B-cells as well as immune-complex-stimulated cytokine production in monocytes, indicating the potential for activity in both the initiation and effector phases of inflammatory arthritis. Furthermore, **68** demonstrated whole blood potency that was superior to that of **1** from our own in vitro studies or from reported clinical studies.¹⁵ In a rat collagen-induced arthritis model where dosing is initiated after the onset of disease, **68** significantly inhibited ankle inflammation when dosed orally at 10, 3, and 1 mg/kg bid (Figure 7A), demonstrating a role for Syk in the effector phase of inflammatory arthritis. There was a direct correlation between exposure and efficacy in this model. To build a correlation of plasma levels, efficacy, and the degree of target inhibition, we developed an in vitro rat whole blood phospho-Syk (pSyk) assay and determined the EC₅₀ for pSyk inhibition to be 1.9 μM . Plasma levels of **68** measured on the final study day (12 h post last dose) were consistent with maintaining 50% (at 3 mg/kg) and 90% (at 10 mg/kg) inhibition of pSyk at trough

(Figure 7B). **68** also showed disease-modifying activity in multiple histological measurements, including inhibition of pannus formation, cartilage damage, bone resorption, and peritosteal bone formation (Figure 7C), with ED₅₀ values ranging from 1.2 to 3.9 mg/kg (Figure 7D). These data suggest that 50% target coverage (pSyk EC₅₀) at trough was sufficient to significantly reduce disease scores.

CONCLUSION

The favorable in vitro and in vivo properties of **68** resulted in its selection as a development candidate, GS-9973. Given the excellent selectivity profile, it is hypothesized that GS-9973 will enable high levels of Syk inhibition clinically with fewer dose-limiting adverse effects associated with more promiscuous inhibitors. GS-9973 is currently being evaluated in human clinical trials.^{41,55}

EXPERIMENTAL SECTION

General Procedures. All commercial reagents were used as provided. Flash chromatography was performed using an ISCO Combiflash Companion purification system with RediSep R_f prepacked silica gel cartridges supplied by Teledyne Isco. ¹H NMR spectra were recorded on a Varian Inova 300 MHz spectrometer. Proton chemical shifts are reported in parts per million from an internal standard or residual solvent. The purity of the tested compounds was assessed to be at least 95% by HPLC analysis unless indicated otherwise. A Gemini C18 110 Å column (50 mm × 4.6 mm, 5 μm particle size) was used with gradient elution of acetonitrile in water, 0–30% for 5 min and then 30–98% for 5 min at a flow rate of 2 mL/min with detection at 254 nm wavelength. For all samples 0.1% TFA was added to both eluents. High-resolution mass spectrometry was performed on an Agilent 6210 time of flight mass spectrometer coupled to an Agilent 1200 rapid resolution HPLC instrument. The samples were run on a Phenomenex Luna C18 column using reversed-phase chromatography with a gradient from 20% to 90% acetonitrile containing 0.1% formic acid. The reference masses that were used during data collection were 118.086255 and 922.009798. Data were processed via Agilent Masshunter B.04 qualitative analysis.

Synthesis of 9. Benzyl 4-Nitrobenzoate (15). A solution of 4-nitrobenzoyl chloride (**14**) (18.6 g, 100 mmol) in methylene chloride (200 mL) was added dropwise to a stirred solution of benzyl alcohol (12.9 g, 120 mmol) and triethylamine (30.3 g, 300 mmol) in methylene chloride (200 mL), and the reaction was stirred at ambient temperature for 22 h. After this time, the reaction was filtered, and the filtrate was washed with brine (400 mL) and then saturated aqueous ammonium chloride (400 mL). The organic layer was dried over sodium sulfate and filtered, and the filtrate was concentrated under reduced pressure. The residue obtained was solvent exchanged with ethanol (200 mL) and then recrystallized from ethanol (150 mL) to afford benzyl 4-nitrobenzoate (20.4 g, 79%) as a light yellow solid: ¹H NMR (300 MHz, CDCl₃) δ 8.30–8.22 (m, 4H), 7.47–7.37 (m, 5H), 5.41 (s, 2H).

Benzyl 4-Aminobenzoate (16). A mixture of **15** (20.4 g, 79.3 mmol) and iron powder (66.4 g, 1190 mmol) in ethanol (600 mL, 1% water) was treated dropwise with a solution of concentrated sulfuric acid (52 mL) in water (204 mL), and the resulting mixture was mechanically stirred at ambient temperature for 1 h. The reaction was treated with additional sulfuric acid (52 mL) and stirred at ambient temperature for 15 min and then at 60 °C for 1.5 h. After this time, the reaction was cooled to ambient temperature and filtered through diatomaceous earth, and the volatiles of the filtrate were removed under reduced pressure. The resulting mixture was extracted with ethyl acetate (500 mL and then 2 × 200 mL), and the combined organics were washed with brine (500 mL). The organic layer was dried over sodium sulfate and filtered, and the filtrate was concentrated under reduced pressure until a small amount of white solid formed, which was removed by filtration. The filtrate was concentrated under reduced

pressure, triturated with heptane (150 mL), dissolved in methylene chloride, and washed with saturated sodium bicarbonate. The organic layer was dried over sodium sulfate and filtered, and the filtrate was concentrated under reduced pressure to afford benzyl 4-amino-benzoate (10.2 g, 57%) as an off-white solid that was used without further purification.

Benzyl 4-(3-(4,4,5,5-Tetramethyl-1,3,2-dioxaborolan-2-yl)-benzamido)benzoate (17). A mixture of **16** (4.39 g, 19.3 mmol), 3-(4,4,5,5-tetramethyl-1,3,2-dioxaborolan-2-yl)benzoyl chloride (4.30 g, 16.1 mmol), and *N,N*-diisopropylethylamine (7.49 g, 57.9 mmol) in methylene chloride (50 mL) was stirred at ambient temperature for 13 h. After this time, the reaction was concentrated under reduced pressure and purified by chromatography (silica, heptane to 1:3 ethyl acetate/heptane) to afford benzyl 4-(3-(4,4,5,5-tetramethyl-1,3,2-dioxaborolan-2-yl)benzamido)benzoate (3.07 g, 78% pure by mass, 27% yield) as a light yellow sticky foam that was used without further purification.

Benzyl 4-(3-(8-((3,4-Dimethoxyphenyl)amino)imidazo[1,2-*a*]pyrazin-6-yl)benzamido)benzoate (18). A mixture of 6-bromo-*N*-(3,4-dimethoxyphenyl)imidazo[1,2-*a*]pyrazin-8-amine (**13**) (1.82 g, 5.22 mmol) and **17** (3.06 g, 5.22 mmol, 78% by mass) in 1 M aqueous sodium carbonate (8 mL) and 1,4-dioxane (24 mL) was sparged with nitrogen with stirring for 5 min. The resulting mixture was treated with tetrakis(triphenylphosphine)palladium(0) (1.20 g, 1.04 mmol) and stirred at reflux for 2.5 h. After this time, the reaction was cooled to ambient temperature, diluted with ethyl acetate (100 mL), and washed with brine (100 mL). The aqueous layer was extracted with ethyl acetate (100 mL), the combined organic layers were dried over sodium sulfate and filtered, and the filtrate was concentrated under reduced pressure. The residue obtained was purified by chromatography (silica, methylene chloride to 1:4 ethyl acetate/methylene chloride) to afford benzyl 4-(3-(8-((3,4-dimethoxyphenyl)amino)imidazo[1,2-*a*]pyrazin-6-yl)benzamido)benzoate (2.02 g, 65%) as an off-white solid: mp 154–160 °C; ¹H NMR (300 MHz, CDCl₃) δ 10.72 (s, 1H), 9.57 (s, 1H), 8.74 (s, 1H), 8.57 (s, 1H), 8.25 (d, *J* = 7.8 Hz, 1H), 8.08–7.94 (m, 7H), 7.69–7.60 (m, 3H), 7.50–7.34 (m, 5H), 6.92 (d, *J* = 8.7 Hz, 1H), 5.36 (s, 2H), 3.78 (s, 3H), 3.73 (s, 3H); ESI MS *m/z* 600 [*M* + *H*]⁺; HPLC 8.93 min, 95.9% (AUC).

4-(3-(8-((3,4-Dimethoxyphenyl)amino)imidazo[1,2-*a*]pyrazin-6-yl)benzamido)benzoic Acid (9). A solution of **18** (1.75 g, 2.92 mmol) in ethyl acetate (500 mL) and ethanol (500 mL) at 60 °C was treated with 10% palladium on carbon (5.11 g, 50% water by weight), sparged with hydrogen for 30 min at 60 °C, and then stirred under balloon pressure hydrogen at 60 °C for 30 min. After this time, the reaction was sparged with nitrogen for 10 min and filtered hot through diatomaceous earth. The filtrate was concentrated under reduced pressure, and the residue obtained was exhaustively triturated (boiling acetonitrile (2 × 50 mL), then boiling methanol (50 mL), then boiling 1:1 methanol/acetonitrile (50 mL), then boiling acetonitrile (50 mL), and then boiling 1:1 methanol/acetonitrile (50 mL)) to afford 4-(3-(8-((3,4-dimethoxyphenyl)amino)imidazo[1,2-*a*]pyrazin-6-yl)benzamido)benzoic acid (458 mg, 31%) as an off-white solid: mp > 250 °C; ¹H NMR (300 MHz, DMSO-*d*₆) δ 12.74 (br s, 1H), 10.67 (s, 1H), 9.57 (s, 1H), 8.74 (s, 1H), 8.56 (s, 1H), 8.25 (d, *J* = 7.8 Hz, 1H), 8.80–7.89 (m, 7H), 7.69–7.53 (m, 3H), 6.93 (d, *J* = 8.7 Hz, 1H), 3.78 (s, 3H), 3.71 (s, 3H); HRMS-ESI⁺ *m/z* calcd for C₂₈H₂₃N₅O₅ 510.1772 (*M* + *H*⁺), found 510.1770 (*M* + *H*⁺).

3-(8-((3,4-Dimethoxyphenyl)amino)imidazo[1,2-*a*]pyrazin-6-yl)benzamide (11). The target compound was obtained following the procedure outlined for **33** as a light green solid (40 mg, 38%): mp 226–228 °C; ¹H NMR (300 MHz, DMSO-*d*₆) δ 9.56 (s, 1H), 8.67 (s, 1H), 8.50 (s, 1H), 8.17 (d, *J* = 7.8 Hz, 1H), 8.10 (d, *J* = 2.4 Hz, 1H), 8.05 (br s, 1H), 8.03 (s, 1H), 7.87 (d, *J* = 7.8 Hz, 1H), 7.68 (m, 1H), 7.59–7.54 (m, 2H), 7.44 (br s, 1H), 6.95 (d, *J* = 8.7 Hz, 1H), 3.82 (s, 3H), 3.76 (s, 3H); ESI MS *m/z* 390 [*M* + *H*]⁺; HRMS *m/z* 390.1577 [*M* + *H*]⁺; HRMS-ESI⁺ *m/z* calcd for C₂₁H₁₉N₅O₃ 390.1561 (*M* + *H*⁺), found 390.1577 (*M* + *H*⁺).

5-(4,4,5,5-Tetramethyl-1,3,2-dioxaborolan-2-yl)-1*H*-indazole (23). A mixture of 5-bromo-1*H*-indazole (**22**) (1.48 g, 7.50 mmol), bis(pinacolato)diboron (2.09 g, 8.25 mmol), and potassium acetate

(2.21 g, 22.5 mmol) in dimethyl sulfoxide (45 mL) was sparged with nitrogen while being stirring for 10 min. Dichloro[1,1'-bis-(diphenylphosphino)ferrocene]palladium(II)–methylene chloride adduct (823 mg, 1.12 mmol) was then added, and the reaction was stirred at 90 °C for 16 h. After this time, the reaction was cooled to room temperature, added to a mixture of 1:1 ethyl acetate/water (400 mL), and sonicated for 5 min. The resulting biphasic mixture was filtered through diatomaceous earth and the filter cake washed with ethyl acetate (50 mL). The layers of the filtrate were separated, and the aqueous phase was extracted with ethyl acetate (2 × 100 mL). The combined organic layers were dried over sodium sulfate, filtered, and concentrated under reduced pressure to afford 5-(4,4,5,5-tetramethyl-1,3,2-dioxaborolan-2-yl)-1H-indazole (667 mg, 36%) as a dark-brown solid that was used without further purification: ESI MS m/z 244.9 $[M + H]^+$.

N-(3,4-Dimethoxyphenyl)-6-(1H-indazol-5-yl)imidazo[1,2-a]pyrazin-8-amine (24). A mixture of 6-bromo-N-(3,4-dimethoxyphenyl)imidazo[1,2-a]pyrazin-8-amine (200 mg, 0.570 mmol), 5-(4,4,5,5-tetramethyl-1,3,2-dioxaborolan-2-yl)-1H-indazole (278 mg, 1.14 mmol), and 1 M aqueous sodium carbonate (1.25 mL) in 1,4-dioxane (4.0 mL) was sparged with nitrogen while being stirred for 5 min. Tetrakis(triphenylphosphine)palladium(0) (66 mg, 0.057 mmol) was then added and the reaction heated under microwave irradiation at 125 °C for 20 min. After this time, the reaction was cooled to room temperature, dissolved in ethyl acetate (10 mL), and filtered through diatomaceous earth. The filtrate was washed with water (20 mL) and then brine (2 × 20 mL) and dried over sodium sulfate. The drying agent was removed by filtration, and the filtrate was concentrated under reduced pressure. The resulting residue was purified by chromatography (silica, gradient, methylene chloride to 1:19 methanol/methylene chloride) to afford N-(3,4-dimethoxyphenyl)-6-(1H-indazol-5-yl)imidazo[1,2-a]pyrazin-8-amine (59 mg, 27%) as an off-white solid: mp > 250 °C; 1H NMR (300 MHz, DMSO- d_6) δ 13.14 (s, 1H), 9.50 (s, 1H), 8.59 (s, 1H), 8.44 (s, 1H), 8.18 (d, J = 2.4 Hz, 1H), 8.14 (s, 1H), 8.01 (m, 2H), 7.62 (m, 3H), 6.98 (d, J = 9.0 Hz, 1H), 3.86 (s, 3H), 3.77 (s, 3H); HRMS-ESI $^+$ m/z calcd for $C_{21}H_{18}N_6O_2$ 387.1564 ($M + H^+$), found 388.1584 ($M + H^+$).

4-Methyl-1-(4-nitrophenyl)piperidin-4-ol (26). A mixture of 1-fluoro-4-nitrobenzene (25) (350 mg, 2.48 mmol), 4-methylpiperidin-4-ol hydrochloride salt (400 mg, 2.64 mmol), and *N,N*-diisopropylethylamine (670 mg, 5.18 mmol) in acetonitrile (6.3 mL) was stirred at reflux for 2.5 h. After this time, the reaction was cooled to room temperature and concentrated under reduced pressure. The resulting residue was purified by chromatography (silica, methylene chloride) to afford 4-methyl-1-(4-nitrophenyl)piperidin-4-ol (441 mg, 75%) as a yellow solid: 1H NMR (300 MHz, DMSO- d_6) δ 8.03–7.99 (m, 2H), 7.01–6.98 (m, 2H), 4.43 (s, 1H), 3.72–3.66 (m, 2H), 3.41–3.30 (m, 2H), 1.56–1.44 (m, 4H), 1.14 (s, 3H).

1-(4-Aminophenyl)-4-methylpiperidin-4-ol (27). A solution of 26 (440 mg, 1.86 mmol) in ethanol (10 mL) and methanol (10 mL) was degassed with nitrogen, and 10% palladium on carbon (50% wet, 170 mg dry weight) was added. The round-bottom flask was charged with hydrogen gas to a pressure of 1 atm, and the contents were stirred for 2.5 h. After this time, the hydrogen gas was evacuated and nitrogen charged into the flask. The catalyst was removed by filtration through a pad of diatomaceous earth and the filter cake washed sequentially with ethyl acetate (30 mL), ethanol (30 mL), and ethyl acetate (30 mL). The filtrate was concentrated under reduced pressure to afford 1-(4-aminophenyl)-4-methylpiperidin-4-ol (373 mg, 97%) as an orange-yellow semisolid that was used in the next step without purification or analysis.

1-(4-((6-Bromoimidazo[1,2-a]pyrazin-8-yl)amino)phenyl)-4-methylpiperidin-4-ol (28). A mixture of 27 (370 mg, 1.79 mmol), 6,8-dibromoimidazo[1,2-a]pyrazine (450 mg, 1.63 mmol), and *N,N*-diisopropylethylamine (420 mg, 3.25 mmol) in 2-propanol (5 mL) was stirred at reflux for 2.5 h and then at room temperature for 18 h. After this time, the mixture was poured into water (20 mL) and stirred for 5 min. The resulting suspension was filtered and the filter cake washed with water (20 mL) and then diethyl ether (20 mL). The filter

cake was dried to a constant weight under vacuum to afford 1-(4-((6-bromoimidazo[1,2-a]pyrazin-8-yl)amino)phenyl)-4-methylpiperidin-4-ol (574 mg, 87%) as a light brown solid: 1H NMR (300 MHz, DMSO- d_6) δ 9.71 (s, 1H), 8.16 (s, 1H), 7.90 (m, 1H), 7.75–7.72 (m, 2H), 7.59 (m, 1H), 6.94–6.91 (m, 2H), 4.25 (s, 1H), 3.30–3.23 (m, 2H), 3.14–3.05 (m, 2H), 1.58–1.54 (m, 4H), 1.51 (s, 3H).

1-(4-((6-(1H-Indazol-6-yl)imidazo[1,2-a]pyrazin-8-yl)amino)phenyl)-4-methylpiperidin-4-ol (30). A mixture of 28 (300 mg, 0.746 mmol) and 6-(4,4,5,5-tetramethyl-1,3,2-dioxaborolan-2-yl)-1H-indazole (29) (270 mg, 1.11 mmol) in 1 M aqueous sodium carbonate (1.5 mL) and 1,4-dioxane (4 mL) was sparged with nitrogen while being stirred for 5 min. Tetrakis(triphenylphosphine)palladium(0) (170 mg, 0.147 mmol) was then added and the reaction heated under microwave irradiation at 135 °C for 35 min. After this time, the reaction was cooled to room temperature, combined with a second lot (0.496 mmol), and filtered through diatomaceous earth and the filter cake washed with ethyl acetate (150 mL). The filtrate was washed with water (30 mL) and then brine (30 mL) and dried over sodium sulfate. The drying agent was removed by filtration and the filtrate concentrated under reduced pressure. The resulting residue was purified by trituration with methanol and then chromatography (silica, gradient, methylene chloride to 19:1 methylene chloride/methanol) to afford 1-(4-((6-(1H-indazol-6-yl)imidazo[1,2-a]pyrazin-8-yl)amino)phenyl)-4-methylpiperidin-4-ol (179 mg, 36% combined) as a light yellow solid: mp >250 °C; 1H NMR (300 MHz, DMSO- d_6) δ 13.17 (s, 1H), 9.45 (s, 1H), 8.65 (s, 1H), 8.19 (s, 1H), 8.08 (s, 1H), 8.00–7.97 (m, 3H), 7.83 (d, J = 8.7 Hz, 1H), 7.72 (d, J = 8.7 Hz, 1H), 7.63 (s, 1H), 6.99 (d, J = 9.0 Hz, 2H), 4.26 (s, 1H), 3.30–3.24 (m, 2H), 3.16–3.07 (m, 2H), 1.60–1.58 (m, 4H), 1.17 (s, 3H); HRMS-ESI $^+$ m/z calcd for $C_{25}H_{25}N_7O$ 440.2193 ($M + H^+$), found 440.2201 ($M + H^+$).

4-Phenyltetrahydro-2H-pyran (32). A solution of aluminum chloride (2.67 g, 20.0 mmol) in anhydrous benzene (50 mL) was cooled to 0 °C in an ice/water bath under a nitrogen atmosphere and treated dropwise with a solution of 4-chlorotetrahydro-2H-pyran (31) (2.11 g, 17.5 mmol) in anhydrous benzene (5 mL). *Caution: gas evolution and exothermic reaction!* When the addition was complete, the cooling bath was removed and the reaction stirred at room temperature for 1 h. After this time, the reaction was poured into a mixture of ice/water (200 mL) and extracted with diethyl ether (200 mL). The organic phase was dried over sodium sulfate and filtered and the filtrate concentrated under reduced pressure to afford 4-phenyltetrahydro-2H-pyran (2.62 g, 92%) as a yellow solid which was used in the next step without purification: 1H NMR (400 MHz, DMSO- d_6) δ 7.29–7.17 (m, 5H), 3.96–3.92 (m, 2H), 3.46–3.40 (m, 2H), 2.84–2.72 (m, 1H), 1.69–1.64 (m, 4H).

4-(4-Nitrophenyl)tetrahydro-2H-pyran (33). A solution of 32 (2.60 g, 16.0 mmol) in glacial acetic acid (15 mL) was treated with a solution of 98% sulfuric acid (0.88 mL) in glacial acetic acid (15 mL), followed by a solution of 90% nitric acid (0.77 mL) in glacial acetic acid (15 mL), and then diluted with 98% sulfuric acid (13.3 mL) and the reaction stirred at room temperature for 30 min. After this time, the mixture was poured into ice/water (50 mL) and slowly treated with sodium bicarbonate (50 g). *Caution: gas evolution and exothermic reaction!* When the addition was complete, the mixture was stirred at 40 °C until gas evolution ceased and then cooled to room temperature. The mixture was brought to pH 14 with 5 M aqueous sodium hydroxide and the resulting suspension filtered. The filtrate was extracted with methylene chloride (3 × 100 mL), and the combined organic layers were dried over sodium sulfate. The drying agent was removed by filtration and the filtrate concentrated under reduced pressure to afford 4-(4-nitrophenyl)tetrahydro-2H-pyran (2.05 g, 62%) as a yellow solid: 1H NMR (400 MHz, DMSO- d_6) δ 8.17 (d, J = 8.8 Hz, 2H), 7.56 (d, J = 8.8 Hz, 2H), 3.98–3.94 (m, 2H), 3.48–3.42 (m, 2H), 3.00–2.92 (m, 1H), 1.74–1.67 (m, 4H).

Methyl 4-(3-(8-((3,4-Dimethoxyphenyl)amino)imidazo[1,2-a]pyrazin-6-yl)benzamido)benzoate (34). A mixture of 3-(8-((3,4-dimethoxyphenyl)amino)imidazo[1,2-a]pyrazin-6-yl)benzoic acid trifluoroacetate salt (500 mg, 0.897 mmol, 70% by mass), methyl 4-aminobenzoate (136 mg, 0.897 mmol), (benzotriazol-1-yloxy)-tripyrrolidinophosphonium hexafluorophosphate (703 mg, 1.35

mmol), and *N,N*-diisopropylethylamine (1.16 g, 8.97 mmol) in DMF (7 mL) was stirred at 60 °C for 14.5 h. After this time, the reaction was diluted with water (100 mL) and extracted with ethyl acetate (100 mL). The organic layer was washed with water (100 mL) and then 5% aqueous lithium chloride (100 mL), dried over sodium sulfate, and filtered, and the filtrate was concentrated under reduced pressure. The residue obtained was purified by chromatography (silica, methylene chloride to 1:39 methanol/methylene chloride) followed by trituration with methylene chloride to afford methyl 4-(3-(8-((3,4-dimethoxyphenyl)amino)imidazo[1,2-*a*]pyrazin-6-yl)benzamido)benzoate (110 mg, 23%) as a white solid: mp 141–144 °C; ¹H NMR (300 MHz, DMSO-*d*₆) δ 10.71 (s, 1H), 9.58 (s, 1H), 8.74 (s, 1H), 8.56 (s, 1H), 8.25 (d, *J* = 7.5 Hz, 1H), 8.08–7.93 (m, 7H), 7.70–7.60 (m, 3H), 6.93 (d, *J* = 8.7 Hz, 1H), 3.85 (s, 3H), 3.77 (s, 3H), 3.71 (s, 3H); HRMS-ESI⁺ *m/z* calcd for C₂₉H₂₅N₅O₅ 524.1928 (M + H⁺), found 524.1954 (M + H⁺).

3-(3-(8-((3,4-Dimethoxyphenyl)amino)imidazo[1,2-*a*]pyrazin-6-yl)benzamido)benzoic Acid (35). The target compound was obtained following the procedure outlined for 33: mp > 250 °C; ¹H NMR (300 MHz, DMSO-*d*₆) δ 10.58 (s, 1H), 9.60 (s, 1H), 8.75 (s, 1H), 8.59 (s, 1H), 8.44 (s, 1H), 8.24 (d, *J* = 7.6 Hz, 1H), 8.08–7.95 (m, 4H), 7.70–7.49 (m, 5H), 6.93 (d, *J* = 8.7 Hz, 1H), 3.78 (s, 3H), 3.71 (s, 3H); HRMS-ESI⁺ *m/z* calcd for C₂₈H₂₃N₅O₅ 510.1722 (M + H⁺), found 510.1783 (M + H⁺).

2-(4-(3-(8-((3,4-Dimethoxyphenyl)amino)imidazo[1,2-*a*]pyrazin-6-yl)benzamido)phenyl)acetic Acid Hydrochloride (36). The target compound was obtained following the procedure outlined for 33 as a yellow solid (68 mg, 84%): mp 176–190 °C; ¹H NMR (300 MHz, DMSO-*d*₆) δ 10.40 (s, 1H), 9.98 (s, 1H), 8.82 (s, 1H), 8.57 (s, 1H), 8.23 (d, *J* = 7.5 Hz, 1H), 8.14 (s, 1H), 8.04 (d, *J* = 2.1 Hz, 1H), 7.97 (d, *J* = 8.1 Hz, 1H), 7.91 (s, 1H), 7.75 (d, *J* = 8.4 Hz, 2H), 7.67 (t, *J* = 7.8 Hz, 1H), 7.59 (dd, *J* = 8.7, 2.4 Hz, 1H), 7.40 (d, *J* = 8.1 Hz, 2H), 6.96 (d, *J* = 8.4 Hz, 1H), 3.79 (s, 3H), 3.72 (s, 3H), 3.56 (s, 2H); HRMS-ESI⁺ *m/z* calcd for C₂₉H₂₅N₅O₅ 524.1928 (M + H⁺), found 524.1939 (M + H⁺).

***N*-(4-(Carbamoylphenyl)-3-(8-((3,4-dimethoxyphenyl)amino)imidazo[1,2-*a*]pyrazin-6-yl)benzamide (37).** A mixture of 4-aminobenzamide (35 mg, 0.256 mmol), *N,N*-diisopropylethylamine (265 mg, 2.05 mmol), 3-(8-((3,4-dimethoxyphenyl)amino)imidazo[1,2-*a*]pyrazin-6-yl)benzoic acid trifluoroacetate salt (145 mg, 0.256 mmol, 69% by mass), and (benzotriazol-1-yloxy)-tripyrrolidinophosphonium hexafluorophosphate (200 mg, 0.384 mmol) in DMF (2 mL) was heated at 75 °C for 2.5 d. After this time, the reaction was concentrated under reduced pressure. The residue obtained was purified twice, first by chromatography (silica, ethyl acetate to 3:7 methanol/methylene chloride) and then by trituration with methanol, to afford *N*-(4-(carbamoylphenyl)-3-(8-((3,4-dimethoxyphenyl)amino)imidazo[1,2-*a*]pyrazin-6-yl)benzamide (15 mg, 12%) as a light brown solid: mp > 250 °C; ¹H NMR (300 MHz, CDCl₃-*d*₆) δ 8.44 (s, 1H), 8.39–7.75 (m, 5H), 7.87–7.75 (m, 3H), 7.64–7.30 (m, 6H), 6.88 (d, *J* = 8.7 Hz, 1H), 3.92 (s, 3H), 3.86 (s, 3H), 1.60 (s, 9H); HRMS-ESI⁺ *m/z* calcd for C₂₈H₂₄N₆O₄ 509.1932 (M + H⁺), found 509.1944 (M + H⁺).

3-(8-((3,4-Dimethoxyphenyl)amino)imidazo[1,2-*a*]pyrazin-6-yl)-*N*-(4-(methylsulfonyl)carbamoylphenyl)benzamide Hydrochloride Salt (38). The target compound was obtained following the procedure outlined for 33 as a yellow solid (44 mg, 18%): mp 228–235 °C; ¹H NMR (300 MHz, CDCl₃) δ 12.03 (br s, 1H), 10.91 (s, 1H), 10.10 (br s, 1H), 8.94 (s, 1H), 8.65 (s, 1H), 8.28–8.25 (m, 1H), 8.15–7.92 (m, 8H), 7.71–7.66 (m, 1H), 7.61–7.59 (m, 1H), 6.97 (d, *J* = 8.7 Hz, 1H), 3.78 (s, 3H), 3.73 (s, 3H), 3.38 (s, 3H); HRMS-ESI⁺ *m/z* calcd for C₂₉H₂₆N₆O₆S 587.1707 (M + H⁺), found 587.1727 (M + H⁺).

***N*-(4-(1*H*-Tetrazol-5-yl)phenyl)-3-(8-((3,4-dimethoxyphenyl)amino)imidazo[1,2-*a*]pyrazin-6-yl)benzamide (39).** The target compound was obtained following the procedure outlined for 33: ¹H NMR (300 MHz, DMSO-*d*₆) δ 10.73 (s, 1H), 9.57 (s, 1H), 8.77 (s, 1H), 8.58 (t, *J* = 1.8 Hz, 1H), 8.29–8.19 (m, 1H), 8.13–7.99 (m, 6H), 7.95 (dt, *J* = 7.9, 1.3 Hz, 1H), 7.71–7.55 (m, 3H), 6.91 (d, *J* = 8.8 Hz,

1H), 3.77 (s, 3H), 3.69 (s, 3H); HRMS-ESI⁺ *m/z* calcd for C₂₈H₂₃N₉O₃ 534.1997 (M + H⁺), found 534.2019 (M + H⁺).

***N*-(4-(1*H*-Imidazol-2-yl)phenyl)-3-(8-((3,4-dimethoxyphenyl)amino)imidazo[1,2-*a*]pyrazin-6-yl)benzamide (40).** The target compound was obtained following the procedure outlined for 33 as a brown solid (50 mg, 40%): mp > 250 °C; ¹H NMR (300 MHz, DMSO-*d*₆) δ 10.52 (s, 1H), 9.58 (s, 1H), 8.74 (s, 1H), 8.57 (s, 1H), 8.24 (d, *J* = 6.6 Hz, 1H), 8.09–7.92 (m, 8H), 7.67–7.61 (m, 3H), 7.19 (s, 2H), 6.94 (d, *J* = 8.7 Hz, 1H), 3.79 (s, 3H), 3.72 (s, 3H); HRMS-ESI⁺ *m/z* calcd for C₃₀H₂₅N₇O₃ 532.2092 (M + H⁺), found 532.2112 (M + H⁺).

***N*-(4-(1*H*-Pyrazol-5-yl)phenyl)-3-(8-((3,4-dimethoxyphenyl)amino)imidazo[1,2-*a*]pyrazin-6-yl)benzamide (41).** The target compound was obtained following the procedure outlined for 33 as an off-white solid (12.2 mg, 13%): mp 250–255 °C; ¹H NMR (300 MHz, DMSO-*d*₆) δ 13.24–12.82 (m, 1H), 10.45 (m, 1H), 9.57 (s, 1H), 8.74 (s, 1H), 8.57 (s, 1H), 8.25 (d, *J* = 8.1 Hz, 1H), 8.09–7.63 (m, 11H), 6.93 (d, *J* = 8.7 Hz, 1H), 6.69 (s, 1H), 3.83 (s, 3H), 3.79 (s, 3H); HRMS-ESI⁺ *m/z* calcd for C₃₀H₂₅N₇O₃ 532.2092 (M + H⁺), found 532.2089 (M + H⁺).

***N*-(4-(1*H*-Pyrazol-4-yl)phenyl)-3-(8-((3,4-dimethoxyphenyl)amino)imidazo[1,2-*a*]pyrazin-6-yl)benzamide (42).** The target compound was obtained following the procedure outlined for 33 as a tan solid (171 mg, 46%): mp > 250 °C; ¹H NMR (300 MHz, DMSO-*d*₆) δ 12.90 (s, 1H), 10.37 (s, 1H), 9.56 (s, 1H), 8.73 (s, 1H), 8.56 (s, 1H), 8.23 (d, *J* = 7.8 Hz, 1H), 8.16–8.09 (m, 2H), 8.03 (s, 1H), 7.94 (m, 2H), 7.80 (d, *J* = 8.4 Hz, 2H), 7.67–7.60 (m, 5H), 6.93 (d, *J* = 8.7 Hz, 1H), 3.79 (s, 3H), 3.72 (s, 3H); HRMS-ESI⁺ *m/z* calcd for C₃₀H₂₅N₇O₃ 532.2092 (M + H⁺), found 532.2087 (M + H⁺).

4-(8-((3,4-Dimethoxyphenyl)amino)imidazo[1,2-*a*]pyrazin-6-yl)benzamide (43). A mixture of (4-(aminocarbonyl)phenyl)boronic acid (114 mg, 0.690 mmol), 6-bromo-*N*-(3,4-dimethoxyphenyl)imidazo[1,2-*a*]pyrazin-8-amine (300 mg, 0.862 mmol), and 1 M aqueous sodium carbonate (1 mL) in 1,4-dioxane (5 mL) was sparged with nitrogen with stirring for 5 min. The reaction was treated with tetrakis(triphenylphosphine)palladium(0) (200 mg, 0.172 mmol) and reacted under microwave irradiation at 135 °C for 15 min. After this time, the reaction was cooled to ambient temperature, and the solids that formed were collected by filtration and triturated with acetonitrile and then methanol to afford 4-(8-((3,4-dimethoxyphenyl)amino)imidazo[1,2-*a*]pyrazin-6-yl)benzamide (96 mg, 36%) as a light-brown solid: mp 248–249 °C; ¹H NMR (300 MHz, DMSO-*d*₆) δ 9.55 (s, 1H), 8.71 (s, 1H), 8.16–7.92 (m, 7H), 7.66 (s, 1H), 7.61 (d, *J* = 8.3 Hz, 1H), 7.39 (s, 1H), 6.97 (d, *J* = 8.6 Hz, 1H), 3.84 (s, 3H), 3.77 (s, 3H); HRMS-ESI⁺ *m/z* calcd for C₃₀H₂₅N₇O₃ 390.1561 (M + H⁺), found 390.1570 (M + H⁺).

3-(8-((3,4-Dimethoxyphenyl)amino)imidazo[1,2-*a*]pyrazin-6-yl)-*N*-methylbenzamide (44). The target compound was obtained following the procedure outlined for 42: ¹H NMR (300 MHz, DMSO-*d*₆) δ 9.54 (s, 1H), 8.64 (s, 1H), 8.54–8.39 (m, 2H), 8.13 (dt, *J* = 7.9, 1.4 Hz, 1H), 8.10 (d, *J* = 2.4 Hz, 1H), 8.00 (d, *J* = 1.1 Hz, 1H), 7.79 (dt, *J* = 7.7, 1.3 Hz, 1H), 7.64 (d, *J* = 1.1 Hz, 1H), 7.59–7.49 (m, 2H), 6.93 (d, *J* = 8.8 Hz, 1H), 3.79 (s, 3H), 3.74 (s, 3H), 3.36–3.23 (m, 1H), 2.81 (d, *J* = 4.5 Hz, 3H); HRMS-ESI⁺ *m/z* calcd for C₂₂H₂₁N₅O₃ 404.1717 (M + H⁺), found 404.1737 (M + H⁺).

3-(8-((3,4-Dimethoxyphenyl)amino)imidazo[1,2-*a*]pyrazin-6-yl)-*N,N*-dimethylbenzamide (45). The target compound was obtained following the procedure outlined for 42: ¹H NMR (300 MHz, DMSO-*d*₆) δ 9.54 (s, 1H), 8.68 (s, 1H), 8.13–8.00 (m, 3H), 7.96 (d, *J* = 1.1 Hz, 1H), 7.64 (d, *J* = 1.1 Hz, 1H), 7.60–7.44 (m, 2H), 7.38 (dt, *J* = 7.6, 1.3 Hz, 1H), 6.93 (d, *J* = 8.8 Hz, 1H), 3.77 (s, 3H), 3.74 (s, 3H), 3.37–3.23 (m, 3H), 3.01 (s, 3H), 2.93 (s, 3H); HRMS-ESI⁺ *m/z* calcd for C₂₃H₂₃N₅O₃ 418.1874 (M + H⁺), found 418.1882 (M + H⁺).

5-(8-((3,4-Dimethoxyphenyl)amino)imidazo[1,2-*a*]pyrazin-6-yl)-2-fluorobenzamide (46). The target compound was obtained following the procedure outlined for 42: mp 232–233 °C; ¹H NMR (300 MHz, DMSO-*d*₆) δ 9.54 (s, 1H), 8.66 (s, 1H), 8.29 (dd, *J* = 6.9, 2.4 Hz, 1H), 8.15–8.09 (m, 1H), 8.06 (d, *J* = 2.4 Hz, 1H), 7.98 (s, 1H), 7.78 (s, 1H), 7.71 (s, 1H), 7.65 (s, 1H), 7.53 (dd, *J* = 8.7, 2.4 Hz,

1H), 7.40 (t, $J = 8.7$ Hz, 1H), 6.94 (d, $J = 8.7$ Hz, 1H), 3.80 (s, 3H), 3.75 (s, 3H); HRMS-ESI⁺ m/z calcd for C₂₁H₁₈FN₅O₃ 408.1466 (M + H⁺), found 408.4188 (M + H⁺).

5-(8-((3,4-Dimethoxyphenyl)amino)imidazo[1,2-*a*]pyrazin-6-yl)-2-methylbenzamide (47). The target compound was obtained following the procedure outlined for 42: mp 243–244 °C; ¹H NMR (300 MHz, DMSO-*d*₆) δ 9.50 (s, 1H), 8.63 (s, 1H), 8.14 (d, $J = 2.4$ Hz, 1H), 8.02 (d, $J = 1.5$ Hz, 1H), 7.98 (s, 1H), 7.94 (dd, $J = 8.1, 1.5$ Hz, 1H), 7.80 (s, 1H), 7.64 (s, 1H), 7.53 (dd, $J = 8.7, 2.4$ Hz, 1H), 7.43 (s, 1H), 7.34 (d, $J = 8.1$ Hz, 1H), 6.94 (d, $J = 8.7$ Hz, 1H), 3.81 (s, 3H), 3.75 (s, 3H), 2.40 (s, 3H); HRMS-ESI⁺ m/z calcd for C₂₂H₂₁N₅O₃ 404.1717 (M + H⁺), found 404.1728 (M + H⁺).

5-(8-((3,4-Dimethoxyphenyl)amino)imidazo[1,2-*a*]pyrazin-6-yl)-2-methoxybenzamide (48). The target compound was obtained following the procedure outlined for 42: mp 228–230 °C dec; ¹H NMR (300 MHz, DMSO-*d*₆) δ 9.58 (s, 1H), 8.60 (s, 1H), 8.44 (s, 1H), 8.11–8.06 (m, 2H), 8.01 (s, 1H), 7.70 (m, 2H), 7.61 (s, 1H), 7.55 (d, $J = 8.7$ Hz, 1H), 7.26 (d, $J = 8.7$ Hz, 1H), 6.94 (d, $J = 8.7$ Hz, 1H), 3.94 (s, 3H), 3.81 (s, 3H), 3.75 (s, 3H); HRMS-ESI⁺ m/z calcd for C₂₂H₂₁N₅O₄ 420.1666 (M + H⁺), found 420.1688 (M + H⁺).

3-(8-((3,4-Dimethoxyphenyl)amino)imidazo[1,2-*a*]pyrazin-6-yl)-4-methylbenzamide (49). The target compound was obtained following the procedure outlined for 42: mp > 250 °C; ¹H NMR (300 MHz, DMSO-*d*₆) δ 9.47 (s, 1H), 8.14 (s, 1H), 8.03–8.00 (m, 2H), 7.95–7.90 (m, 2H), 7.81 (dd, $J = 8.1, 1.7$ Hz, 1H), 7.66 (s, 1H), 7.55 (dd, $J = 8.7, 2.3$ Hz, 1H), 7.39 (d, $J = 8.1$ Hz, 1H), 7.30 (bs, 1H), 6.88 (d, $J = 8.7$ Hz, 1H), 3.70 (s, 3H), 3.68 (s, 3H), 2.47 (s, 3H); HRMS-ESI⁺ m/z calcd for C₂₂H₂₁N₅O₃ 404.1717 (M + H⁺), found 404.1735 (M + H⁺).

4-(8-((3,4-Dimethoxyphenyl)amino)imidazo[1,2-*a*]pyrazin-6-yl)-2-fluorobenzamide (50). The target compound was obtained following the procedure outlined for 42: mp > 250 °C; ¹H NMR (300 MHz, DMSO-*d*₆) δ 9.60 (s, 1H), 8.77 (s, 1H), 8.04 (d, $J = 2.1$ Hz, 1H), 7.99 (s, 1H), 7.92–7.87 (m, 2H), 7.81–7.75 (m, 1H), 7.70–7.65 (m, 3H), 7.56 (dd, $J = 8.7, 2.1$ Hz, 1H), 6.97 (d, $J = 8.7$ Hz, 1H), 3.84 (s, 3H), 3.76 (s, 3H); HRMS-ESI⁺ m/z calcd for C₂₁H₁₈FN₅O₃ 408.1466 (M + H⁺), found 408.1479 (M + H⁺).

4-(8-((3,4-Dimethoxyphenyl)amino)imidazo[1,2-*a*]pyrazin-6-yl)-2-methylbenzamide (51). The target compound was obtained following the procedure outlined for 42: mp 225–237 °C; ¹H NMR (300 MHz, DMSO-*d*₆) δ 9.52 (s, 1H), 8.64 (s, 1H), 8.11 (d, $J = 2.3$ Hz, 1H), 7.99–7.98 (m, 1H), 7.92–7.84 (m, 2H), 7.74 (bs, 1H), 7.65–7.64 (m, 1H), 7.57 (dd, $J = 8.7, 2.3$ Hz, 1H), 7.48 (d, $J = 7.9$ Hz, 1H), 7.36 (bs, 1H), 6.97 (d, $J = 8.7$ Hz, 1H), 3.83 (s, 3H), 3.76 (s, 3H), 2.45 (s, 3H); HRMS-ESI⁺ m/z calcd for C₂₂H₂₁N₅O₃ 404.1717 (M + H⁺), found 404.1718 (M + H⁺).

4-(8-((3,4-Dimethoxyphenyl)amino)imidazo[1,2-*a*]pyrazin-6-yl)-2-methoxybenzamide (52). The target compound was obtained following the procedure outlined for 42: mp 221–222 °C dec; ¹H NMR (300 MHz, DMSO-*d*₆) δ 9.56 (s, 1H), 8.75 (s, 1H), 7.99 (d, $J = 1.2$ Hz, 1H), 7.92 (d, $J = 8.1$ Hz, 1H), 7.87 (d, $J = 2.4$ Hz, 1H), 7.77–7.66 (m, 5H), 7.54 (bs, 1H), 6.97 (d, $J = 8.7$ Hz, 1H), 4.01 (s, 3H), 3.79 (s, 3H), 3.76 (s, 3H); HRMS-ESI⁺ m/z calcd for C₂₂H₂₁N₅O₄ 420.1666 (M + H⁺), found 420.1681 (M + H⁺).

4-(8-((3,4-Dimethoxyphenyl)amino)imidazo[1,2-*a*]pyrazin-6-yl)-3-methylbenzamide (53). The target compound was obtained following the procedure outlined for 42: mp 238–241 °C; ¹H NMR (300 MHz, DMSO-*d*₆) δ 9.48 (s, 1H), 8.15 (s, 1H), 8.01–7.98 (m, 2H), 7.86–7.76 (m, 3H), 7.66–7.58 (m, 3H), 7.36 (bs, 1H), 6.89 (d, $J = 8.7$ Hz, 1H), 3.71 (s, 6H), 2.50 (s, 3H); HRMS-ESI⁺ m/z calcd for C₂₂H₂₁N₅O₃ 404.1717 (M + H⁺), found 404.1736 (M + H⁺).

N-(3,4-Dimethoxyphenyl)-6-(1H-indol-6-yl)imidazo[1,2-*a*]pyrazin-8-amine (54). The target compound was obtained following the procedure outlined for 23: mp 215–217 °C; ¹H NMR (300 MHz, DMSO-*d*₆) δ 11.23 (s, 1H), 9.45 (s, 1H), 8.53 (s, 1H), 8.12 (d, $J = 2.4$ Hz, 1H), 8.08 (s, 1H), 7.98 (s, 1H), 7.67–7.59 (m, 4H), 7.39 (t, $J = 2.7$ Hz, 1H), 6.97 (d, $J = 8.7$ Hz, 1H), 6.45 (m, 1H), 3.82 (s, 3H), 3.76 (s, 3H); HRMS-ESI⁺ m/z calcd for C₂₂H₁₉N₅O₂ 386.1612 (M + H⁺), found 386.1630 (M + H⁺).

N-(3,4-Dimethoxyphenyl)-6-(1H-indazol-6-yl)imidazo[1,2-*a*]pyrazin-8-amine (55). The target compound was obtained following

the procedure outlined for 23: mp 250–252 °C; ¹H NMR (300 MHz, DMSO-*d*₆) δ 13.12 (s, 1H), 9.46 (s, 1H), 8.61 (s, 1H), 8.13 (s, 1H), 8.02–8.01 (m, 2H), 7.94 (d, $J = 0.9$ Hz, 1H), 7.77 (d, $J = 8.4$ Hz, 1H), 7.68 (dd, $J = 8.4, 0.9$ Hz, 1H), 7.58 (d, $J = 0.9$ Hz, 1H), 7.55 (dd, $J = 8.4, 2.4$ Hz, 1H), 6.91 (d, $J = 8.4$ Hz, 1H), 3.76 (s, 3H), 3.71 (s, 3H); HRMS-ESI⁺ m/z calcd for C₂₁H₁₈N₆O₂ 387.1564 (M + H⁺), found 387.1579 (M + H⁺).

6-(1H-Benzo[d]imidazol-5-yl)-N-(3,4-dimethoxyphenyl)-imidazo[1,2-*a*]pyrazin-8-amine (56). The target compound was obtained following the procedure outlined for 23: mp 135–137 °C; ¹H NMR (300 MHz, DMSO-*d*₆) δ 12.58 (s, 0.5H), 12.51 (s, 0.5H), 9.48 (s, 1H), 8.60 (s, 1H), 8.34–8.10 (m, 3H), 7.98 (s, 1H), 7.91–7.82 (m, 1H), 7.73–7.62 (m, 3H), 6.97 (d, $J = 9.0$ Hz, 1H), 3.87 (s, 1.5H), 3.82 (s, 1.5H), 3.77 (s, 3H); HRMS-ESI⁺ m/z calcd for C₂₁H₁₈N₆O₂ 387.1564 (M + H⁺), found 387.1578 (M + H⁺).

6-(1H-Benzo[d][1,2,3]triazol-6-yl)-N-(3,4-dimethoxyphenyl)-imidazo[1,2-*a*]pyrazin-8-amine (57). The target compound was obtained following the procedure outlined for 23: mp 244–250 °C; ¹H NMR (300 MHz, DMSO-*d*₆) δ 9.54 (s, 1H), 8.71 (s, 1H), 8.49 (s, 1H), 8.10 (d, $J = 2.4$ Hz, 1H), 8.03–7.94 (m, 3H), 7.65 (s, 1H), 7.61 (dd, $J = 8.7, 2.4$ Hz, 1H), 6.98 (d, $J = 8.7$ Hz, 1H), 3.85 (s, 3H), 3.77 (s, 3H); HRMS-ESI⁺ m/z calcd for C₂₀H₁₇N₇O₂ 388.1516 (M + H⁺), found 388.1515 (M + H⁺).

N-(3,4-Dimethoxyphenyl)-6-(1H-indol-5-yl)imidazo[1,2-*a*]pyrazin-8-amine (58). The target compound was obtained following the procedure outlined for 23: mp 235–237 °C; ¹H NMR (300 MHz, DMSO-*d*₆) δ 11.17 (s, 1H), 9.43 (s, 1H), 8.51 (s, 1H), 8.26 (m, 2H), 7.96 (d, $J = 0.9$ Hz, 1H), 7.75 (dd, $J = 8.7, 1.5$ Hz, 1H), 7.61 (d, $J = 0.9$ Hz, 1H), 7.57 (dd, $J = 8.7, 2.4$ Hz, 1H), 7.47 (d, $J = 8.7$ Hz, 1H), 7.38 (t, $J = 2.4$ Hz, 1H), 6.97 (d, $J = 8.7$ Hz, 1H), 6.47 (m, 1H), 3.87 (s, 3H), 3.76 (s, 3H); HRMS-ESI⁺ m/z calcd for C₂₂H₁₉N₅O₂ 386.1612 (M + H⁺), found 388.1616 (M + H⁺).

N-(3,4-Dimethoxyphenyl)-6-(1-methyl-1H-indazol-6-yl)-imidazo[1,2-*a*]pyrazin-8-amine (59). The target compound was obtained following the procedure outlined for 23: mp 185–187 °C; ¹H NMR (300 MHz, DMSO-*d*₆) δ 9.55 (s, 1H), 8.71 (s, 1H), 8.22 (s, 1H), 8.10–8.07 (m, 2H), 8.02 (s, 1H), 7.83 (m, 2H), 7.67 (s, 1H), 7.67–7.64 (m, 1H), 6.99 (d, $J = 8.7$ Hz, 1H), 4.12 (s, 3H), 3.83 (s, 3H), 3.77 (s, 3H); HRMS-ESI⁺ m/z calcd for C₂₂H₂₀N₆O₂ 401.1721 (M + H⁺), found 401.1726 (M + H⁺).

N-(3,4-Dimethoxyphenyl)-6-(1-methyl-1H-indazol-5-yl)-imidazo[1,2-*a*]pyrazin-8-amine (60). The target compound was obtained following the procedure outlined for 23: mp 210–212 °C; ¹H NMR (300 MHz, DMSO-*d*₆) δ 9.51 (s, 1H), 8.62 (s, 1H), 8.43 (s, 1H), 8.18 (d, $J = 2.4$ Hz, 1H), 8.12 (s, 1H), 8.05 (dd, $J = 9.0, 1.5$ Hz, 1H), 7.98 (s, 1H), 7.74 (d, $J = 9.0$ Hz, 1H), 7.64 (s, 1H), 7.60 (dd, $J = 9.0, 2.4$ Hz, 1H), 6.99 (d, $J = 9.0$ Hz, 1H), 4.09 (s, 3H), 3.87 (s, 3H), 3.77 (s, 3H); HRMS-ESI⁺ m/z calcd for C₂₂H₂₀N₆O₂ 401.1721 (M + H⁺), found 401.1739 (M + H⁺).

6-(8-((3,4-Dimethoxyphenyl)amino)imidazo[1,2-*a*]pyrazin-6-yl)-2H-benzo[b][1,4]oxazin-3(4H)-one (61). The target compound was obtained following the procedure outlined for 23: mp 235–237 °C; ¹H NMR (300 MHz, DMSO-*d*₆) δ 10.94 (s, 1H), 9.46 (s, 1H), 8.41 (s, 1H), 7.99 (s, 1H), 7.91 (d, $J = 2.1$ Hz, 1H), 7.74 (dd, $J = 8.7, 2.1$ Hz, 1H), 7.62 (s, 1H), 7.56–7.51 (m, 2H), 7.04 (d, $J = 8.7$ Hz, 1H), 6.98 (d, $J = 8.7$ Hz, 1H), 4.62 (s, 2H), 3.78 (s, 3H), 3.77 (s, 3H); HRMS-ESI⁺ m/z calcd for C₂₂H₁₉N₅O₄ 418.1510 (M + H⁺), found 418.1512 (M + H⁺).

7-(8-((3,4-Dimethoxyphenyl)amino)imidazo[1,2-*a*]pyrazin-6-yl)-2H-benzo[b][1,4]oxazin-3(4H)-one (62). The target compound was obtained following the procedure outlined for 23: mp > 250 °C; ¹H NMR (300 MHz, DMSO-*d*₆) δ 10.81 (s, 1H), 9.48 (s, 1H), 8.53 (s, 1H), 8.04 (d, $J = 2.4$ Hz, 1H), 7.94 (s, 1H), 7.62–7.56 (m, 4H), 6.99–6.95 (m, 2H), 4.62 (s, 2H), 3.82 (s, 3H), 3.75 (s, 3H); HRMS-ESI⁺ m/z calcd for C₂₂H₁₉N₅O₄ 418.1510 (M + H⁺), found 418.1499 (M + H⁺).

6-(3,4-Dihydro-2H-benzo[b][1,4]oxazin-6-yl)-N-(3,4-dimethoxyphenyl)imidazo[1,2-*a*]pyrazin-8-amine (63). The target compound was obtained following the procedure outlined for 23: mp 179–182 °C; ¹H NMR (300 MHz, DMSO-*d*₆) δ 9.39 (s, 1H),

8.32 (s, 1H), 8.01 (d, $J = 2.4$ Hz, 1H), 7.95 (s, 1H), 7.67 (dd, $J = 8.7$, 2.4 Hz, 1H), 7.59 (s, 1H), 7.23 (d, $J = 2.1$ Hz, 1H), 7.11 (dd, $J = 8.4$, 2.1 Hz, 1H), 6.96 (d, $J = 8.7$ Hz, 1H), 6.72 (d, $J = 8.4$ Hz, 1H), 5.86 (m, 1H), 4.16 (m, 2H), 3.80 (s, 3H), 3.75 (s, 3H), 3.33 (m, 2H, merged with H₂O peak); HRMS-ESI⁺ m/z calcd for C₂₂H₂₁N₅O₃ 404.1717 (M + H⁺), found 404.1728 (M + H⁺).

6-(1H-Indazol-6-yl)-N-phenylimidazo[1,2-*a*]pyrazin-8-amine (64). The target compound was obtained following the procedure outlined for **29**: mp > 250 °C; ¹H NMR (300 MHz, DMSO-*d*₆) δ 13.20 (bs, 1H), 9.69 (s, 1H), 8.74 (s, 1H), 8.20–8.18 (m, 3H), 8.09 (s, 1H), 8.03 (d, $J = 0.9$ Hz, 1H), 7.85 (d, $J = 8.7$ Hz, 1H), 7.73 (dd, $J = 8.7$, 1.2 Hz, 1H), 7.68 (d, $J = 1.2$ Hz, 1H), 7.41 (m, 2H), 7.08 (t, $J = 6.9$ Hz, 1H); HRMS-ESI⁺ m/z calcd for C₁₉H₁₄N₆ 327.1353 (M + H⁺), found 327.1362 (M + H⁺).

6-(1H-Indazol-6-yl)-N-(3-methoxyphenyl)imidazo[1,2-*a*]pyrazin-8-amine (65). The target compound was obtained following the procedure outlined for **29**: mp 238–240 °C; ¹H NMR (300 MHz, DMSO-*d*₆) δ 13.21 (s, 1H), 9.66 (s, 1H), 8.73 (s, 1H), 8.18 (s, 1H), 8.10 (s, 1H), 8.05–8.03 (m, 2H), 7.85 (d, $J = 8.4$ Hz, 1H), 7.76–7.72 (m, 2H), 7.71 (s, 1H), 7.28 (t, $J = 8.4$ Hz, 1H), 6.63 (dd, $J = 8.4$, 2.1 Hz, 1H), 3.81 (s, 3H); HRMS-ESI⁺ m/z calcd for C₂₀H₁₆N₆O 357.1458 (M + H⁺), found 357.1477 (M + H⁺).

6-(1H-Indazol-6-yl)-N-(4-methoxyphenyl)imidazo[1,2-*a*]pyrazin-8-amine (66). The target compound was obtained following the procedure outlined for **29**: mp > 250 °C; ¹H NMR (300 MHz, DMSO-*d*₆) δ 13.17 (s, 1H), 9.57 (s, 1H), 8.68 (s, 1H), 8.18 (s, 1H), 8.08 (s, 1H), 8.06 (d, $J = 9.0$ Hz, 2H), 7.99 (d, $J = 0.9$ Hz, 1H), 7.84 (d, $J = 8.4$ Hz, 1H), 7.72 (dd, $J = 8.4$, 1.2 Hz, 1H), 7.64 (d, $J = 0.9$ Hz, 1H), 6.99 (d, $J = 9.0$ Hz, 2H), 3.79 (s, 3H); HRMS-ESI⁺ m/z calcd for C₂₀H₁₆N₆O 357.1458 (M + H⁺), found 357.1477 (M + H⁺).

1-(4-((6-(1H-Indazol-6-yl)imidazo[1,2-*a*]pyrazin-8-yl)amino)phenyl)-3-methylazetidin-3-ol (67). The target compound was obtained following the procedure outlined for **29**: mp 265–268 °C dec; ¹H NMR (300 MHz, DMSO-*d*₆) δ 13.18 (s, 1H), 9.38 (s, 1H), 8.63 (s, 1H), 8.17 (s, 1H), 8.08 (s, 1H), 7.97–7.93 (m, 3H), 7.83 (d, $J = 8.4$ Hz, 1H), 7.71 (d, $J = 8.4$ Hz, 1H), 7.62 (s, 1H), 6.52 (d, $J = 8.7$ Hz, 2H), 5.47 (s, 1H), 3.77 (d, $J = 7.5$ Hz, 2H), 3.61 (d, $J = 7.5$ Hz, 2H), 1.48 (s, 3H); HRMS-ESI⁺ m/z calcd for C₂₃H₂₁N₇O 412.1880 (M + H⁺), found 412.1884 (M + H⁺).

6-(1H-Indazol-6-yl)-N-(4-morpholinophenyl)imidazo[1,2-*a*]pyrazin-8-amine (68). The target compound was obtained following the procedure outlined for **29**: mp > 250 °C; ¹H NMR (300 MHz, DMSO-*d*₆) δ 13.17 (s, 1H), 9.50 (s, 1H), 8.66 (s, 1H), 8.19 (s, 1H), 8.09 (s, 1H), 8.03 (d, $J = 8.7$ Hz, 2H), 7.99 (d, $J = 0.9$ Hz, 1H), 7.84 (d, $J = 8.7$ Hz, 1H), 7.72 (dd, $J = 8.7$, 0.9 Hz, 1H), 7.63 (d, $J = 0.9$ Hz, 1H), 7.00 (d, $J = 8.7$ Hz, 2H), 3.77 (t, $J = 4.6$ Hz, 4H), 3.11 (t, $J = 4.6$ Hz, 4H); HRMS-ESI⁺ m/z calcd for C₂₃H₂₁N₇O 412.1880 (M + H⁺), found 412.1894 (M + H⁺).

6-(1H-Indazol-6-yl)-N-(4-(dioxothiomorpholino)phenyl)imidazo[1,2-*a*]pyrazin-8-amine (69). The target compound was obtained following the procedure outlined for **29**: mp > 250 °C; ¹H NMR (300 MHz, DMSO-*d*₆) δ 13.17 (s, 1H), 9.57 (s, 1H), 8.67 (s, 1H), 8.18 (s, 1H), 8.09–8.06 (m, 3H), 7.99 (d, $J = 1.2$ Hz, 1H), 7.84 (d, $J = 8.4$ Hz, 1H), 7.72 (dd, $J = 8.4$, 1.2 Hz, 1H), 7.64 (d, $J = 0.9$ Hz, 1H), 7.08 (d, $J = 9.0$ Hz, 2H), 3.76–3.74 (m, 4H), 3.18–3.16 (m, 4H); HRMS-ESI⁺ m/z calcd for C₂₃H₂₁N₇O₂S: 460.1550 (M + H⁺), found 460.1557 (M + H⁺).

6-(1H-Indazol-6-yl)-N-(4-(tetrahydro-2H-pyran-4-yl)phenyl)imidazo[1,2-*a*]pyrazin-8-amine (70). The target compound was obtained following the procedure outlined for **29** using nitro reagent **32** in the second step: mp > 300 °C; ¹H NMR (400 MHz, DMSO-*d*₆) δ 13.19 (s, 1H), 9.64 (s, 1H), 8.71 (s, 1H), 8.20 (s, 1H), 8.12 (d, $J = 8.8$ Hz, 2H), 8.09 (s, 1H), 8.01 (d, $J = 0.8$ Hz, 1H), 7.85 (d, $J = 8.4$ Hz, 1H), 7.73 (dd, $J = 8.4$, 1.2 Hz, 1H), 7.66 (d, $J = 0.8$ Hz, 1H), 7.28 (d, $J = 8.8$ Hz, 2H), 3.99–3.96 (m, 2H), 3.49–3.43 (m, 2H), 2.81–2.76 (m, 1H), 1.75–1.65 (m, 4H); HRMS-ESI⁺ m/z calcd for C₂₄H₂₂N₆O 411.1928 (M + H⁺), found 411.1930 (M + H⁺).

2-((4-((6-(1H-Indazol-6-yl)imidazo[1,2-*a*]pyrazin-8-yl)amino)phenyl)methylamino)ethanol (71). The target compound was obtained following the procedure outlined for **29**: mp 229–231 °C; ¹H NMR (300 MHz, DMSO-*d*₆) δ 13.18 (bs, 1H), 9.33 (s, 1H), 8.62

(s, 1H), 8.18 (s, 1H), 8.08 (s, 1H), 7.97–7.92 (m, 3H), 7.83 (d, $J = 8.4$ Hz, 1H), 7.71 (dd, $J = 8.4$, 0.9 Hz, 1H), 7.62 (d, $J = 0.9$ Hz, 1H), 6.77 (d, $J = 9.3$ Hz, 2H), 4.64 (t, $J = 5.1$ Hz, 1H), 3.60–3.56 (m, 2H), 3.40 (t, $J = 6.3$ Hz, 2H), 2.95 (s, 3H); HRMS-ESI⁺ m/z calcd for C₂₂H₂₁N₇O 400.1880 (M + H⁺), found 400.1892 (M + H⁺).

N-(4-(1,4-Oxazepan-4-yl)phenyl)-6-(1H-indazol-6-yl)-imidazo[1,2-*a*]pyrazin-8-amine (72). The target compound was obtained following the procedure outlined for **29**: mp 237–240 °C; ¹H NMR (300 MHz, DMSO-*d*₆) δ 13.17 (s, 1H), 9.35 (s, 1H), 8.61 (s, 1H), 8.17 (s, 1H), 8.08 (s, 1H), 7.97–7.93 (m, 3H), 7.82 (d, $J = 8.4$ Hz, 1H), 7.71 (d, $J = 8.4$ Hz, 1H), 7.61 (s, 1H), 6.79 (d, $J = 9.0$ Hz, 2H), 3.75 (t, $J = 4.5$ Hz, 2H), 3.61–3.58 (m, 6H), 1.94 (t, $J = 5.7$ Hz, 2H); HRMS-ESI⁺ m/z calcd for C₂₄H₂₃N₇O 426.2037 (M + H⁺), found 426.2049 (M + H⁺).

6-(1H-Indazol-6-yl)-N-(3-methoxy-4-morpholinophenyl)-imidazo[1,2-*a*]pyrazin-8-amine (73). The target compound was obtained following the procedure outlined for **29** using 3-methoxy-4-morpholinoaniline in the coupling step: mp > 250 °C; ¹H NMR (300 MHz, DMSO-*d*₆) δ 13.19 (s, 1H), 9.55 (s, 1H), 8.69 (s, 1H), 8.21 (s, 1H), 8.09–8.08 (m, 2H), 8.00 (s, 1H), 7.84 (d, $J = 8.7$ Hz, 1H), 7.75 (d, $J = 8.7$ Hz, 1H), 7.67–7.65.

Kinase Assays. Full-length baculovirus-expressed Syk (Cell Signaling Technologies, Danver, MA) kinase activity was measured in a Lance-based assay format in a final volume of 25 μ L containing 25 mM Tris-HCl, pH 7.5, 5 mM β -glycerophosphate, 2 mM DTT, 0.1 mM Na₃VO₄, 10 mM MgCl₂, 0.5 μ M Promega PTK biotinylated peptide substrate 1, 0.01% casein, 0.01% Triton X-100, 0.25% glycerol, and 40 mM ATP (K_m for ATP) incubated at room temperature for 60 min. Reactions were stopped with the addition of 30 mM EDTA containing 30 μ L of SA-APC and 4 nM PT-66 antibody and the plates measured on a Perkin-Elmer Envision. IC₅₀ values for test compounds were determined using a four-parameter linear regression algorithm.

DiscoverX Screen. Compounds were screened at 10 μ M in the KINOMEScan (DiscoverX, San Diego, CA) assay, and the results for the primary screen binding interactions are reported as “percent control”, where lower numbers indicate stronger hits in the matrix. Values of >35% are considered “no hits”. K_d determinations were assessed at DiscoverX.

Cellular Cross-Screening Activity Assays. Bone marrow derived mouse mast cells (BMMCs), HUVECs, or SK-N-MCs were resuspended at (1–2) $\times 10^6$ cells/wells in Tyrode’s buffer (BMMCs) or RPMI and incubated with compound dilutions for 1 h followed by stimulation with 50 ng/mL SCF (BMMCs), 50 ng/mL VEGF (HUVECs), or 100 ng/mL GDNF (SK-N-MCs). Following 3–15 min of stimulation, the cells were washed in PBS and resuspended in cell lysis buffer (Cell Signaling) and the proteins resolved by SDS-PAGE. Immunodetection was evaluated for phospho-cKit (Cell Signaling) in the BMMCs and normalized to total PLC γ 2 (Santa Cruz Biotechnology, Santa Cruz, CA), phospho-KDR (Cell Signaling) in HUVECs, and phospho-Ret (Cell Signaling) in SK-N-MCs. Detection was enabled by the use of infrared-conjugated secondary antibodies and Odyssey software (LiCor Biosciences, Lincoln, NE).

Jak2 Activity Assay. TF1 cells were serum starved overnight in 1% fetal bovine serum (FBS) RPMI medium at 1 $\times 10^6$ cells/mL. Cells were resuspended in fresh serum-free RPMI and incubated with compound dilutions for 1 h followed by stimulation with 5 units/mL erythropoietin (R&D Systems, Minneapolis, MN). The cells were lysed in 50 μ L of RIPA buffer, and phospho-Stat5 was detected using an MSD phospho-Stat5 quantitation plate (Meso Scale Discovery, Rockville, MD).

MV-4-11 Proliferation Assays. Functional impact on cellular Flt3 activity was determined by measuring compound inhibition of MV-4-11 (ATCC no. CRL-9591) cell proliferation. A total of 10⁴ cells were diluted in RPMI medium containing 10% FBS in 96-well flat-bottomed tissue culture plates and incubated with compound dilutions for 72 h at 37 °C. Alamar blue (10%) was added to the cells, which were incubated for an additional 12–18 h at 37 °C, and inhibition of the relative cell numbers was determined by spectrophotometer readings at 570/600 nm.

Ramos Assay (pBLNK). Ramos cells were serum starved at 2×10^6 cells/mL in serum-free RPMI for 1 h in an upright T175 Falcon TC flask. The cells were centrifuged (1100 rpm for 5 min) and incubated at a density of 5×10^6 cells/mL in the presence of 3 \times serial dilutions of test compound or DMSO controls for 1 h at 37 °C. The cells were stimulated by incubation with 3 μ g/mL antihuman IgM F(ab)₂ (Southern Biotech, Birmingham, AL) for 5 min at 37 °C. The cells were pelleted and lysed in 50 μ L of cell lysis buffer. Phospho-BLNK was detected using an MSD high bind plate coated for 1 h with 30 ng/well total BLNK capture antibody (Santa Cruz Biotechnology). Lysate was added, and the cells were washed in TBS–1% Tween-20 and probed with an antiphospho-Blnk-Y96 antibody (Santa Cruz Biotechnology). Inhibition of the pBLNK was quantitated versus the control well (Meso Scale Discovery).

Human CD86 Expression. Isolated human B-cells (Stem Cell Technologies, Vancouver, Canada) were thawed briefly in a 37 °C water bath and plated in RPMI 1640 medium supplemented with 10% FBS, 100 units/mL penicillin–streptomycin, 0.01 M HEPES, 2 mM GlutaMAX, 5 mM sodium pyruvate, and 10 mM β -mercaptoethanol at a density of 5×10^5 cells/200 μ L per well of a flat-bottom 96-well plate. The cells were incubated with compound for 1 h in a 37 °C incubator with 5% CO₂ and stimulated with 20 μ g/mL mouse F(ab')₂ antihuman IgM in the continued presence of compound for 16 h. The cells were washed two times in PBS + 4% FBS and then stained with 20 μ L each of anti-CD19 and anti-CD86 and 2.5 μ L 7AAD for 40 min on ice. The cells were pelleted at 300g for 5 min, washed three times with PBS + 4% FBS, and analyzed by flow cytometry.

Human B-Cell Proliferation. Isolated human B-cells (Stem Cell Technologies) were thawed in a 37 °C water bath and rested in RPMI 1640 medium supplemented with 10% FBS, 100 units/mL penicillin–streptomycin, 0.01 M HEPES, 2 mM GlutaMAX, 5 mM sodium pyruvate, and 10 mM β -mercaptoethanol for 5 h in a 37 °C incubator with 5% CO₂ and subsequently loaded with 5 μ M CFSE per the manufacturer's instructions (Life Technologies, Carlsbad, CA). The cells (3×10^5 cells/200 μ L per well) in a round-bottom 96-well plate were incubated with compound for 1 h in a 37 °C incubator, then stimulated with 20 μ g/mL goat F(ab')₂ antihuman IgM and 20 μ g/mL mouse anti-CD40, and incubated for 90 h in a 37 °C incubator. The cells were rinsed once in PBS + 4% FBS and incubated with 7AAD for 30 min on ice. The cells were pelleted at 300g for 10 min, rinsed twice, and analyzed by flow cytometry on the 7AAD⁺ population, and proliferation was estimated on the basis of the reduction of fluoroscein staining.

Immune-Complex Stimulation of TNF α Production. Frozen human monocytes (Stem Cell Technologies) were quickly thawed in a 37 °C water bath and rested for 3 h at 37 °C in RPMI 1640 medium supplemented with 10% heat-inactivated FBS, 2 mM Glutamax, 1 \times sodium pyruvate, 0.1 M HEPES, 10 mM β -mercaptoethanol, and 100 units/mL penicillin–streptomycin prior to plating in 96-well plates at 1×10^5 cells/well in 100 μ L of complete RPMI. The cells were incubated with compound for 1 h and stimulated with 4 μ L of immune complex at 40 μ g/mL (stock solution of 300 μ L of a polyclonal goat F(ab')₂ antihuman F_c + 35 μ L of purified human IgG + 65 μ L of medium (final mass ratio of 3:1) incubated on ice for 1 h prior to use) for 16 h at 37 °C. Culture supernatants were harvested and stored at –20 °C until they were analyzed for TNF α levels using a singleplex Meso Scale TNF α kit (Meso Scale Discovery).

CD63 Whole Blood Assay. Fresh human whole blood was collected in sodium heparin vacutainers (catalog no. 367874, BD Biosciences, San Jose, CA). A 2 μ L sample of compound in 2 \times serial dilutions was added to 100 μ L of whole blood in a 96-well microtiter plate and incubated for 1 h at 37 °C. A 20 μ L sample of antihuman IL-3 potentiation buffer B (catalog no. 10-0500, Glycotope Biotechnology GmbH, Heidelberg, Germany) was added for 10 min at 37 °C, followed by goat antihuman IgE (catalog no. H15700, Invitrogen, Chicago, IL) stimulation for 20 min at 37 °C. The reaction was placed on ice to stop degranulation, and the cells were stained with 20 μ L of anti-CD63-FITC/anti-CD123-PE/anti-HLA-DR-PerCEP (catalog no. 341068, Becton, Dickinson and Co., Pasadena, CA). Red blood cells were lysed with 1.6 mL of buffer G for 10 min and protected from

light, and cell pellets were harvested by centrifugation at 1300 rpm for 10 min at RT. The pellets were washed one time with 1.0 mL of wash buffer A for 5 min and recentrifuged. CD63 expression on CD123+/HLA– cells was measured by fluorescence-activated cell sorting (FACS) analysis on a Canto FACS Calibur (BD Biosciences), and the CD63 expression (%) versus DMSO controls was used to determine the EC₅₀ in whole blood.

Rat Collagen-Induced Arthritis (CIA) Model. Female Lewis rats from Charles River (mean mass 178 g, eight per group for collagen arthritis, four per group for normal controls) were anesthetized with isoflurane and injected with 300 μ L of Freund's incomplete adjuvant (Difco, Detroit, MI) containing 2 mg/mL bovine type II collagen (Elastin Products, Owensville, MI) at the base of the tail and two sites on the back on days 0 and 6. Oral dosing (bid at 12 h intervals) was performed on arthritic days 0–7 with vehicle (Cremophor/ethanol/saline), GS-9973 (1, 3, or 10 mg/kg), or the reference compound dexamethasone (Dex; 0.075 mg/kg) administered daily (qd). Rats were terminated on arthritis day 16. Efficacy evaluation was based on animal body masses, daily ankle caliper measurements, ankle diameters expressed as the area under the curve (AUC), terminal hind paw masses, and histopathologic evaluation of ankles and knees. PK was measured from plasma samples taken 0, 2, 4, 8, 12, and 24 h post last dose. The paws were fixed in formalin and processed for hematoxylin (H) and eosin (E) microscopy. H and E sections were scored for bone resorption as follows: (0) normal; (0.5) normal on low magnification but have the earliest hint of small areas of resorption in the metaphysis with no resorption in the tarsal bones; (1) (minimal) small definite areas of resorption in distal tibial trabecular or cortical bone or in the tarsal bones, not readily apparent on low magnification, rare osteoclasts; (2) (mild) more numerous areas (<25% loss of bone in growth plate area) of resorption in distal tibial trabecular or cortical bone and tarsals apparent on low magnification, osteoclasts more numerous; (3) (moderate) obvious resorption of medullary trabecular and cortical bone without full thickness defects in both distal tibial cortices, loss of some medullary trabeculae with 26–50% loss across the growth plate and cortices, some loss in tarsal bones, lesion apparent on low magnification, osteoclasts more numerous; (4) (marked) full or nearly full thickness defects in both distal tibial cortices, often with distortion of the profile of the remaining cortical surface, marked loss of medullary bone of distal tibia (50–100% loss across the growth plate area and cortices and up to 50% loss in small tarsals if minor in tibia), numerous osteoclasts, minor to mild resorption in smaller tarsal bones; (5) (severe) full thickness defects in both distal tibial cortices with >75% loss across the growth plate and both cortices and >50% loss in tarsals, often with distortion of the profile of the remaining cortical surface, marked loss of medullary bone of distal tibia, numerous osteoclasts. Osteoclast counts (5400 \times fields) were performed on the ankles in the areas of greatest bone resorption. For statistical analysis, the ankle thicknesses, bone erosion scores, osteoclast counts, and c-fos expression values (mean \pm SE) were analyzed for group differences using the Student's *t* test. Significance was set at *p* < 0.05.

Competitive Protein Binding Assay. Human plasma and cell culture medium containing 10% fetal bovine serum (CCM) were spiked with the test compound at a final concentration of 2 μ M. Spiked plasma (1 mL) and CCM (1 mL) were placed into opposite sides of the assembled dialysis cells, which were separated by a semipermeable membrane. The dialysis cells were rotated slowly in a 37 °C water bath for the time necessary to reach equilibrium. Postdialysis plasma and CCM masses were measured, and the test compound concentrations in plasma and CCM were determined with LC/MS/MS.

Metabolic Stability. Metabolic stability in vitro was determined using pooled hepatic microsomal fractions (final protein concentration of 0.5 mg/mL) at a final test compound concentration of 3 μ M. The reaction was initiated by the addition of an NADPH-regenerating system. An aliquot of 25 μ L of the reaction mixture was transferred at various time points to plates containing a quenching solution. The test compound concentration in the reaction mixture was determined with

LC/MS/MS. Predicted clearance was calculated using the well-stirred liver model without protein restriction.

Metabolic stability was also determined in cryopreserved hepatocytes using tritiated test compounds. The incubation mixture contained 1×10^6 hepatocytes/mL and 1 μ M tritiated test compound (2.5 μ Ci). The incubation was carried out with gentle shaking at 37 °C under a humid atmosphere of 95% air/5% CO₂ (v/v). Aliquots of 50 μ L were removed after 0, 1, 3, and 6 h and added to 100 μ L of quenching solution. The samples were analyzed on a flow scintillation radio detector coupled to an HPLC system. The metabolites were quantified on the basis of the peak areas from the radio detector with the cell-free control samples used as a reference. Metabolic stabilities in hepatocytes were determined by measuring the rate of disappearance of the test compound as a percentage of the total peak area of the formed radiolabeled metabolites and the test compound.

Pharmacokinetics. Pharmacokinetic studies were performed in male naive Sprague–Dawley (SD) rats, non-naive beagle dogs, and cynomolgus monkeys (three animals per dosing route) following federal and Institutional Animal Care and Use Committee (IACUC) guidelines. Intravenous (iv) administration was dosed via infusion over 30 min in a vehicle containing 5% ethanol, 20% PEG400, and 75% water (pH adjusted to 3.0 with HCl). Oral dosing was administered by gavage in a vehicle containing 5% ethanol, 45% PEG 400, and 50% 50 mM citrate buffer, pH 3. Blood samples were collected over a 24 h period postdose into Vacutainer tubes containing EDTA-K2. Plasma was isolated, and the concentration of the test compound in plasma was determined with LC/MS/MS after protein precipitation with acetonitrile.

Noncompartmental pharmacokinetic analysis was performed on plasma concentration data to calculate pharmacokinetic parameters using the software program WinNonLin (version 5.0.1).

■ ASSOCIATED CONTENT

● Supporting Information

DiscoverX primary screen data and selectivity scores for GS-9973. This material is available free of charge via the Internet at <http://pubs.acs.org>.

Accession Codes

The PDB code for compound **9** bound to Syk is 4PV0, and that for compound **68** bound to Syk is 4PUZ.

■ AUTHOR INFORMATION

Corresponding Author

*Phone: 203-315-7459. E-mail: scotta.mitchell@gilead.com.

Notes

The authors declare no competing financial interest.

■ ACKNOWLEDGMENTS

We thank Kathy Brendza and Loredana Serafini for generating HRMS data, Jayaraman Chandrasekhar for modeling input, Will Watkins and Gregory Notte for manuscript review, and Douglas Stafford for chemistry outsourcing management at Albany Molecular Research Institute (AMRI).

■ ABBREVIATIONS USED

Syk, spleen tyrosine kinase; ITAM, immunoreceptor tyrosine-based activation motif; BLNK, B-cell linker protein; RA, rheumatoid arthritis; TNF α , tumor necrosis factor α ; ITP, idiopathic thrombocytopenia purpura; SLE, systemic lupus erythematosis; AHA, autoimmune hemolytic anemia; SAR, structure–activity relationship; BCR, B-cell receptor; DTT, dithiothreitol; BMMC, bone marrow-derived mast cell; HUVEC, human umbilical vein endothelial cell; SCF, stem cell factor; FACS, fluorescence-activated cell sorting

■ REFERENCES

- (1) Mocsai, A.; Ruland, J.; Tybulewicz, V. L. The SYK tyrosine kinase: a crucial player in diverse biological functions. *Nat. Rev. Immunol.* **2010**, *10*, 387–402.
- (2) Tan, S. L.; Liao, C.; Lucas, M. C.; Stevenson, C.; Demartino, J. A. Targeting the SYK-BTK axis for the treatment of immunological and hematological disorders: recent progress and therapeutic perspectives. *Pharmacol. Ther.* **2013**, *138*, 294–309.
- (3) Alinari, L.; Christian, B.; Baiocchi, R. A. Novel targeted therapies for mantle cell lymphoma. *Oncotarget* **2012**, *3*, 203–11.
- (4) Kurosaki, T. Molecular mechanisms in B cell antigen receptor signaling. *Curr. Opin. Immunol.* **1997**, *9*, 309–318.
- (5) Kurosaki, T. Molecular dissection of B cell antigen receptor signaling. *Int. J. Mol. Med.* **1998**, *1*, 515–527.
- (6) Kurosaki, T.; Johnson, S. A.; Pao, L.; Sada, K.; Yamamura, H.; Cambier, J. C. Role of the Syk autophosphorylation site and SH2 domains in B cell antigen receptor signaling. *J. Exp. Med.* **1995**, *182*, 1815–1823.
- (7) Toapanta, F. R.; Bernal, P. J.; Szein, M. B. Diverse phosphorylation patterns of B cell receptor-associated signaling in naive and memory human B cells revealed by phosphoflow, a powerful technique to study signaling at the single cell level. *Front. Cell. Infect. Microbiol.* **2012**, *2*, 128.
- (8) Baba, Y.; Hashimoto, S.; Matsushita, M.; Watanabe, D.; Kishimoto, T.; Kurosaki, T.; Tsukada, S. BLNK mediates Syk-dependent Btk activation. *Proc. Natl. Acad. Sci. U.S.A.* **2001**, *98*, 2582–2586.
- (9) Rivera, J.; Colbert, R. A. Healing the Syk through kinase inhibitors. *N. Engl. J. Med.* **2010**, *363*, 1362–1364.
- (10) Navarro-Millan, I.; Curtis, J. R. Newest clinical trial results with antitumor necrosis factor and nonantitumor necrosis factor biologics for rheumatoid arthritis. *Curr. Opin. Rheumatol.* **2013**, *25*, 384–390.
- (11) Sullivan, S. D.; Alfonso-Cristancho, R.; Carlson, J.; Mallya, U.; Ringold, S. Economic consequences of sequencing biologics in rheumatoid arthritis: a systematic review. *J. Med. Econ.* **2013**, *16*, 391–396.
- (12) Ruzza, P.; Biondi, B.; Calderan, A. Therapeutic prospect of Syk inhibitors. *Expert Opin. Ther. Pat.* **2009**, *19*, 1361–1376.
- (13) Moretto, A. F.; Dehnhardt, C.; Kaila, N.; Papaioannou, N.; Thorarensen, A. The 2010 patent landscape for spleen tyrosine kinase inhibitors. *Recent Pat. Inflammation Allergy Drug Discovery* **2012**, *6*, 97–120.
- (14) Singh, R.; Masuda, E. S.; Payan, D. G. Discovery and development of spleen tyrosine kinase (SYK) inhibitors. *J. Med. Chem.* **2012**, *55*, 3614–3643.
- (15) Braselmann, S.; Taylor, V.; Zhao, H.; Wang, S.; Sylvain, C.; Baluom, M.; Qu, K.; Herlaar, E.; Lau, A.; Young, C.; Wong, B. R.; Lovell, S.; Sun, T.; Park, G.; Argade, A.; Jurcevic, S.; Pine, P.; Singh, R.; Grossbard, E. B.; Payan, D. G.; Masuda, E. S. R406, an orally available spleen tyrosine kinase inhibitor blocks fc receptor signaling and reduces immune complex-mediated inflammation. *J. Pharmacol. Exp. Ther.* **2006**, *319*, 998–1008.
- (16) Coffey, G.; DeGuzman, F.; Inagaki, M.; Pak, Y.; Delaney, S. M.; Ives, D.; Betz, A.; Jia, Z. J.; Pandey, A.; Baker, D.; Hollenbach, S. J.; Phillips, D. R.; Sinha, U. Specific inhibition of spleen tyrosine kinase suppresses leukocyte immune function and inflammation in animal models of rheumatoid arthritis. *J. Pharmacol. Exp. Ther.* **2012**, *340*, 350–359.
- (17) Liddle, J.; Atkinson, F. L.; Barker, M. D.; Carter, P. S.; Curtis, N. R.; Davis, R. P.; Douault, C.; Dickson, M. C.; Elwes, D.; Garton, N. S.; Gray, M.; Hayhow, T. G.; Hobbs, C. I.; Jones, E.; Leach, S.; Leavens, K.; Lewis, H. D.; McCleary, S.; Neu, M.; Patel, V. K.; Preston, A. G.; Ramirez-Molina, C.; Shipley, T. J.; Skone, P. A.; Smithers, N.; Somers, D. O.; Walker, A. L.; Watson, R. J.; Weingarten, G. G. Discovery of GSK143, a highly potent, selective and orally efficacious spleen tyrosine kinase inhibitor. *Bioorg. Med. Chem. Lett.* **2011**, *21*, 6188–6194.
- (18) Liao, C.; Hsu, J.; Kim, Y.; Hu, D.-Q.; Xu, D.; Zhang, J.; Pachine, A.; Menke, J.; Whittard, T.; Romero, N.; Truitt, T.; Slade, M.; Lukacs,

- C.; Hermann, J.; Zhou, M.; Lucas, M.; Narula, S.; DeMartino, J.; Tan, S.-L. Selective inhibition of spleen tyrosine kinase (SYK) with a novel orally bioavailable small molecule inhibitor, RO9021, impinges on various innate and adaptive immune responses: implications for SYK inhibitors in autoimmune disease therapy. *Arthritis Res. Ther.* **2013**, *15* (R146), 1–14.
- (19) Cha, H. S.; Boyle, D. L.; Inoue, T.; Schoot, R.; Tak, P. P.; Pine, P.; Firestein, G. S. A novel spleen tyrosine kinase inhibitor blocks c-Jun N-terminal kinase-mediated gene expression in synovial cells. *J. Pharmacol. Exp. Ther.* **2006**, *317*, 571–578.
- (20) Norman, P. Evaluation of WO2011134971, chiral 1,6-naphthyridine Syk kinase inhibitors. *Expert Opin. Ther. Pat.* **2012**, *22*, 335–339.
- (21) Pine, P. R.; Chang, B.; Schoettler, N.; Banquerigo, M. L.; Wang, S.; Lau, A.; Zhao, F.; Grossbard, E. B.; Payan, D. G.; Braun, E. Inflammation and bone erosion are suppressed in models of rheumatoid arthritis following treatment with a novel Syk inhibitor. *Clin. Immunol.* **2007**, *124*, 244–257.
- (22) Bahjat, F. R.; Pine, P. R.; Reitsma, A.; Cassafer, G.; Baluom, M.; Grillo, S.; Chang, B.; Zhao, F. F.; Payan, D. G.; Grossbard, E. B.; Daikh, D. I. An orally bioavailable spleen tyrosine kinase inhibitor delays disease progression and prolongs survival in murine lupus. *Arthritis Rheum.* **2008**, *58*, 1433–1444.
- (23) Deng, G. M.; Liu, L.; Bahjat, F. R.; Pine, P. R.; Tsokos, G. C. Suppression of skin and kidney disease by inhibition of spleen tyrosine kinase in lupus-prone mice. *Arthritis Rheum.* **2010**, *62*, 2086–2092.
- (24) Smith, J.; McDaid, J. P.; Bhangal, G.; Chawanasuntorapoj, R.; Masuda, E. S.; Cook, H. T.; Pusey, C. D.; Tam, F. W. A spleen tyrosine kinase inhibitor reduces the severity of established glomerulonephritis. *J. Am. Soc. Nephrol.* **2010**, *21*, 231–236.
- (25) Colonna, L.; Catalano, G.; Chew, C.; D'Agati, V.; Thomas, J. W.; Wong, F. S.; Schmitz, J.; Masuda, E. S.; Reizis, B.; Tarakhovsky, A.; Clynes, R. Therapeutic targeting of Syk in autoimmune diabetes. *J. Immunol.* **2010**, *185*, 1532–1543.
- (26) Podolanczuk, A.; Lazarus, A. H.; Crow, A. R.; Grossbard, E.; Bussel, J. B. Of mice and men: an open-label pilot study for treatment of immune thrombocytopenic purpura by an inhibitor of Syk. *Blood* **2009**, *113*, 3154–3160.
- (27) Matsubara, S.; Koya, T.; Takeda, K.; Joetham, A.; Miyahara, N.; Pine, P.; Masuda, E. S.; Swasey, C. H.; Gelfand, E. W. Syk activation in dendritic cells is essential for airway hyperresponsiveness and inflammation. *Am. J. Respir. Cell Mol. Biol.* **2006**, *34*, 426–433.
- (28) Matsubara, S.; Li, G.; Takeda, K.; Loader, J. E.; Pine, P.; Masuda, E. S.; Miyahara, N.; Miyahara, S.; Lucas, J. J.; Dakhama, A.; Gelfand, E. W. Inhibition of spleen tyrosine kinase prevents mast cell activation and airway hyperresponsiveness. *Am. J. Respir. Crit. Care Med.* **2006**, *173*, 56–63.
- (29) Fruchon, S.; Kheirallah, S.; Al Saati, T.; Ysebaert, L.; Laurent, C.; Leseux, L.; Fournie, J. J.; Laurent, G.; Bezombes, C. Involvement of the Syk-mTOR pathway in follicular lymphoma cell invasion and angiogenesis. *Leukemia* **2012**, *26*, 795–805.
- (30) Suljagic, M.; Longo, P. G.; Bennardo, S.; Perlas, E.; Leone, G.; Laurenti, L.; Efremov, D. G. The Syk inhibitor fostamatinib disodium (R788) inhibits tumor growth in the Emu- TCL1 transgenic mouse model of CLL by blocking antigen-dependent B-cell receptor signaling. *Blood* **2010**, *116*, 4894–4905.
- (31) Young, R. M.; Hardy, I. R.; Clarke, R. L.; Lundy, N.; Pine, P.; Turner, B. C.; Potter, T. A.; Refaeli, Y. Mouse models of non-Hodgkin lymphoma reveal Syk as an important therapeutic target. *Blood* **2009**, *113*, 2508–2516.
- (32) Morales-Torres, J. The status of fostamatinib in the treatment of rheumatoid arthritis. *Expert Rev. Clin. Immunol.* **2012**, *8*, 609–615.
- (33) Fleischmann, R.; Cutolo, M.; Genovese, M. C.; Lee, E. B.; Kanik, K. S.; Sadis, S.; Connell, C. A.; Gruben, D.; Krishnaswami, S.; Wallenstein, G.; Wilkinson, B. E.; Zwillich, S. H. Phase IIb dose-ranging study of the oral JAK inhibitor tofacitinib (CP-690,550) or adalimumab monotherapy versus placebo in patients with active rheumatoid arthritis with an inadequate response to disease-modifying antirheumatic drugs. *Arthritis Rheum.* **2012**, *64*, 617–629.
- (34) Weinblatt, M. E.; Kavanaugh, A.; Burgos-Vargas, R.; Dikranian, A. H.; Medrano-Ramirez, G.; Morales-Torres, J. L.; Murphy, F. T.; Musser, T. K.; Straniero, N.; Vicente-Gonzales, A. V.; Grossbard, E. Treatment of rheumatoid arthritis with a Syk kinase inhibitor: a twelve-week, randomized, placebo-controlled trial. *Arthritis Rheum.* **2008**, *58*, 3309–3318.
- (35) Weinblatt, M. E.; Kavanaugh, A.; Genovese, M. C.; Musser, T. K.; Grossbard, E. B.; Magilavy, D. B. An oral spleen tyrosine kinase (Syk) inhibitor for rheumatoid arthritis. *N. Engl. J. Med.* **2013**, *363*, 1303–1312.
- (36) AstraZeneca. AstraZeneca announces top-line results from phase III OSKIRA trials of FOSTAMATINIB and decision not to proceed with regulatory filings. <http://www.astrazeneca.com/Media/Press-releases/Article/20130504-astrazeneca-announces-topline-results-from-phase-iii-o>; press release, June 4, 2013.
- (37) AstraZeneca. AstraZeneca announces top-line results of OSKIRA-4 phase IIb study of fostamatinib as a monotherapy for rheumatoid arthritis. <http://www.astrazeneca.com/Media/Press-releases/Article/20121213-AstraZeneca-announces-results-OSKIRA-4-study-fostamatinib>; press release, December 13, 2012.
- (38) AstraZeneca. AstraZeneca announces top-line results from OSKIRA-1 phase III study of fostamatinib in rheumatoid arthritis. <http://www.astrazeneca.com/Media/Press-releases/Article/20130405--astrazeneca-announces-topline-results-from-oskira1>; press release, April 5, 2013.
- (39) Friedberg, J. W.; Sharman, J.; Sweetenham, J.; Johnston, P. B.; Vose, J. M.; Lacasce, A.; Schaefer-Cuttillo, J.; De Vos, S.; Sinha, R.; Leonard, J. P.; Cripe, L. D.; Gregory, S. A.; Sterba, M. P.; Lowe, A. M.; Levy, R.; Shipp, M. A. Inhibition of Syk with fostamatinib disodium has significant clinical activity in non-Hodgkin lymphoma and chronic lymphocytic leukemia. *Blood* **2010**, *115*, 2578–2585.
- (40) Park, S. R.; Speranza, G.; Piekarz, R.; Wright, J. J.; Kinders, R. J.; Wang, L.; Pfister, T.; Trepel, J. B.; Lee, M. J.; Alarcon, S.; Steinberg, S. M.; Collins, J.; Doroshow, J. H.; Kummer, S. A multi-histology trial of fostamatinib in patients with advanced colorectal, non-small cell lung, head and neck, thyroid, and renal cell carcinomas, and pheochromocytomas. *Cancer Chemother. Pharmacol.* **2013**, *71*, 981–990.
- (41) Jin, F.; DiPaolo, J. A.; Shao-Li, X.; Yellin, O.; Hawkins, M. J.; Ramanathan, S. Evaluation of the safety, pharmacokinetics and pharmacodynamics of GS-9973, a novel SYK inhibitor, and GS-1101, a novel PI3K δ inhibitor, when administered alone or in combination in humans. Presented at the 104th Annual Meeting of the American Association for Cancer Research, Washington, DC, Apr 6–10, 2013.
- (42) McAdoo, S. P.; Tam, F. W. Fostamatinib disodium. *Drugs Future* **2011**, *36*, 273.
- (43) Krishnan, S.; Juang, Y. T.; Chowdhury, B.; Magilavy, A.; Fisher, C. U.; Nguyen, H.; Nambiar, M. P.; Kyttaris, V.; Weinstein, A.; Bahjat, R.; Pine, P.; Rus, V.; Tsokos, G. C. Differential expression and molecular associations of Syk in systemic lupus erythematosus T cells. *J. Immunol.* **2008**, *181*, 8145–8152.
- (44) Mitchell, S. A.; Currie, K. S.; Blomgren, P. A.; Kropf, J. E.; Lee, S. H.; Xu, J.; Stafford, D. G.; Harding, J. P.; Barbosa Jr, A. J.; Zhao, Z. PCT Int. Appl. WO2010068257, 2010.
- (45) Yamamoto, N.; Takeshita, K.; Shichijo, M.; Kokubo, T.; Sato, M.; Nakashima, K.; Ishimori, M.; Nagai, H.; Li, Y.-F.; Yura, T.; Bacon, K. B. The orally available spleen tyrosine kinase inhibitor 2-[7-(3,4-dimethoxyphenyl)-imidazo-[1,2-c]pyrimidine-5-ylamino]-nicotinamide dihydrochloride (BAY 61-3606) blocks antigen-induced airway inflammation in rats. *J. Pharm. Exp. Ther.* **2003**, *306*, 1174–1181.
- (46) Davis, M. I.; Hunt, J. P.; Herrgard, S.; Cicci, P.; Wodicka, L. M.; Pallares, G.; Hocker, M.; Treiber, D. K.; Zarrinkar, P. P. Comprehensive analysis of kinase inhibitor selectivity. *Nat. Biotechnol.* **2011**, *29*, 1046–1051.
- (47) Karaman, M. W.; Herrgard, S.; Treiber, D. K.; Gallant, P.; Atteridge, C. E.; Campbell, B. T.; Chan, K. W.; Cicci, P.; Davis, M. I.; Edeen, P. T.; Faraoni, R.; Floyd, M.; Hunt, J. P.; Lockhart, D. J.; Milanov, Z. V.; Morrison, M. J.; Pallares, G.; Patel, H. K.; Pritchard, S.;

Wodicka, L. M.; Zarrinkar, P. P. A quantitative analysis of kinase inhibitor selectivity. *Nat. Biotechnol.* **2008**, *26*, 127–132.

(48) Patani, G. A.; LaVoie, E. J. Bioisosterism: a rational approach in drug design. *Chem. Rev.* **1996**, *96*, 3147–3176.

(49) Ballatore, C.; Hury, D. M.; Smith, A. B., III. Carboxylic acid (bio)isosteres in drug design. *ChemMedChem* **2013**, *8*, 385–395.

(50) Herr, R. J. 5-Substituted-1H-tetrazoles as carboxylic acid isosteres: medicinal chemistry and synthetic methods. *Bioorg. Med. Chem.* **2002**, *10*, 3379–3393.

(51) Lucas, M. C.; Goldstein, D. M.; Hermann, J. C.; Kuglstat, A.; Liu, W.; Luk, K. C.; Padilla, F.; Slade, M.; Villaseñor, A. G.; Wanner, J.; Xie, W.; Zhang, X.; Liao, C. Rational design of highly selective spleen tyrosine kinase inhibitors. *J. Med. Chem.* **2012**, *55*, 10414–10423.

(52) Tu, M.; Rai, B. K.; Mathiowetz, A. M.; Didiuk, M.; Pfefferkorn, J. A.; Guzman-Perez, A.; Benbow, J.; Guimarães, C. R. W.; Mente, S.; Hayward, M. M. Exploring aromatic chemical space with NEAT: novel and electronically equivalent aromatic template. *J. Chem. Inf. Model.* **2012**, *52*, 1114–1123.

(53) Villaseñor, A. G.; Kondru, R.; Ho, H.; Wang, S.; Papp, E.; Shaw, D.; Barnett, J. W.; Browner, J. W.; Kuglstat, A. Structural insights for design of potent spleen tyrosine kinase inhibitors from crystallographic analysis of three inhibitor complexes. *Chem. Biol. Drug Des.* **2009**, *73*, 466–470.

(54) Harris, P. A.; Bloor, A.; Cheung, M.; Kumar, R.; Crosby, R. M.; Davis-Ward, R. G.; Epperly, A. H.; Hinkle, K. W.; Hunter, R. N., 3rd; Johnson, J. H.; Knick, V. B.; Laudeman, C. P.; Luttrell, D. K.; Mook, R. A.; Nolte, R. T.; Rudolph, S. K.; Szewczyk, J. R.; Truesdale, A. T.; Veal, J. M.; Wang, L.; Stafford, J. A. Discovery of 5-[[4-[(2,3-dimethyl-2H-indazol-6-yl)methylamino]-2-pyrimidinyl]amino]-2-methyl-benzene-sulfonamide (pazopanib), a novel and potent vascular endothelial growth factor receptor inhibitor. *J. Med. Chem.* **2008**, *51*, 4632–4640.

(55) Ramanathan, S.; DiPaolo, J. A.; Doan, T.; Burge, D. Single and multiple dose-ranging evaluation of safety, pharmacokinetics, and pharmacodynamics of GS-9973, a novel pSYK inhibitor. Presented at the 104th Annual Meeting of the American Association for Cancer Research, Washington, DC, Apr 6–10, 2013.